Filomat 38:10 (2024), 3597–3626
https://doi.org/10.2298/FIL2410597K

Published by Faculty of Sciences and Mathematics,
University of Niš, Serbia
Available at: http://www.pmf.ni.ac.rs/filomat

Dynamical analysis of a predator-prey model in toxic environment with strong reproductive Allee effect

Souvick Karmakar[a], Parvez Akhtar[a], Debgopal Sahoo[a], Guruprasad Samanta[a,*]

[a]*Department of Mathematics, Indian Institute of Engineering Science and Technology, Shibpur, Howrah - 711103, India*

Abstract. In theoretical ecology, the interaction between predator and prey is a natural phenomenon that greatly influences how communities are organized and how ecological diversity is preserved. In ecology, the effect of toxicity on predator and prey population is a quite important topic nowadays. In this current work, we have taken a look at a Gause-type predator-prey model with a simplified Holling type IV functional response and a strong Allee effect on the prey population. The effects of toxicity on both predator and prey species have also been introduced. The feasibility and stability requirements of all equilibrium points are properly examined in terms of model parameters. The parametric restrictions of at least one interior equilibrium point have been derived, and the outcomes are illustrated numerically. It is demonstrated that the system undergoes local bifurcations such as transcritical bifurcation, saddle-node bifurcation, Hopf bifurcation, Bogdanov-Takens bifurcation and cusp bifurcation. The basin of attraction of the proposed system is also demonstrated in this study. Numerous numerical examples are used to support each of these theoretical conclusions.

1. Introduction

Predator-prey interactions are fundamental ecological relationships that impact the dynamics of ecosystems. Organisms from various links of the food chain engage in an intricate act of survival through one species that plays the role of the predator while pursuing, killing, and consuming another species that plays the role of the prey. This intricate relationship has far-reaching implications for population dynamics, species distribution, and even evolutionary adaptations [5, 20]. Predator and prey interactions are crucial in managing population levels, with abundant prey causing higher predator population. Expanding predator population leads to food shortages, resulting in a cyclical balance. Predator-prey interaction models have been studied during the last few decades in order to gain insight the dynamics of numerous intervening species. The value of modeling various events in real-life circumstances is enormous [1, 6, 18]. In the year 1920, predator-prey modeling was first introduced. The Lotka-Volterra Model [12, 30], which was proposed in 1925, essentially a two-species interaction model in an eco-system, was the first notable study in the modeling of predator-prey interaction. Later on, this model was utilized to construct a large variety

2020 *Mathematics Subject Classification*. Primary 92B05; Secondary 92D25, 92D40
Keywords. Prey-predator model; Toxic effect; Allee effect; Holling type IV functional response; Local bifurcation; Basin of attraction.
Received: 22 August 2023; Accepted: 10 September 2023
Communicated by Maria Alessandra Ragusa
Research supported by Indian Institute of Engineering Science and Technology, Shibpur
* Corresponding author: Guruprasad Samanta
Email addresses: skarmakaruttarpara@gmail.com (Souvick Karmakar), pakhtardream@gmail.com (Parvez Akhtar), debgopalsahoo94@gmail.com (Debgopal Sahoo), g_p_samanta@yahoo.co.uk, gpsamanta@math.iiests.ac.in (Guruprasad Samanta)

of models in the ecological system. Several researchers are still attempting to improve the model in order to overcome flaws and get a better understanding of interaction. If we examine the ideas underlying such modeling carefully, we will see that the growth function of prey and the functional response of predators play a very important role.

Functional response is a key concept in mathematical ecology that defines how a predator's consumption rate changes in response to changes in prey size. It depicts the link between the size of prey encountered and its consumption rate. Although appearing in three distinct patterns regulating predation intensity, the complex functional response mechanism manifests itself in three primary types. Understanding functional response is crucial for forecasting population dynamics in ecological systems and to gain knowledge of predator-prey dynamics. Appropriate functional responses are used to explain the impact of corresponding ecological models. Among those various functional responses, some are Lotka-Volterra, Michaelis-Menten, Monod functional response [7, 9, 10, 14, 26, 29] which are used frequently. The predator-prey relation between wolves (Canis lupus) and moose (Alces alces) in North America's boreal woods is a typical example of Holling type II functional response. Wolves have better access to prey when the moose population increases, resulting in an increase in the rate of predation. This interaction, however, approaches a saturation level at which the predation rate plateaus, showing that wolves are restricted by various constraints other than prey density, such as social structure or accessible predation regions [13]. The bright colours of poison dart frogs act as warning signals to prospective predators. Toxic alkaloid substances secreted by these frogs through their skin can be deadly or cause serious diseases in predators. The toxicity of these frogs is assumed to be derived from their diet of poisonous chemicals-containing ants and mites [21]. Also, in another way, we can think that if any prey population gets affected by toxicity, then they will die because of that toxin. Besides this, the predators, who attack and consume those infected prey may also have a chance to get affected. Thus their(predator) population can also be decreased.

These experimental results encourage researchers to enhance the predator-prey model by introducing toxicity into the prey population [19, 24]. In nature, the population of prey makes a special effort to reach areas where they will be secured from predators. Such refuges often serve to decrease the likelihood of extinction of prey owing to predator ingestion as well as to dump prey-predator oscillations [3, 23, 28]. The prey also tries to keep themselves safe from those places or substances that might cause disease or toxicity to them.

Holling categorized functional responses into three categories: Type I, Type II, and Type III. Each category denotes a distinct relationship between the predator's consuming rate and the population size of prey. The Type I functional response presupposes that the predator's consuming rate and prey population size have a linear relationship. In this kind, as prey population size rises, the predator's consumption rate rises steadily until it reaches its carrying capacity. Once the handling capacity is achieved, the feeding rate, despite of the amount of prey, remains constant. But in Holling type II functional response, predator consumption rate initially rises linearly with prey population size. However, these rates gradually level out and become close to an upper limit. Due to the S-shaped curve, it is called a "sigmoidal" response. This shows that the predator's eating rate rises as prey population size rises but declines as predator abundance rises. This kind of behaviour is frequently seen in predators with slow reaction times or ineffective hunting abilities. Type III functional response is distinguished by a modest initial rise in consumption rate in response to prey population size, followed by fast acceleration and subsequently leveling out. Due to problems in detecting and catching prey, this type implies that the predator's eating rate is poor at low prey population size. As the population size of the prey population rises, however, the predators become increasingly adept at locating and seizing their prey. This results in a sharp increase in the rate of consumption [8].

The sigmoid functional response, commonly referred to as Holling Type IV, is a mathematical model used in ecology to explain the connection between a predator's consumption rate and the population size of its prey. C.S. Holling proposed this as one of the functional response types in his research on interactions between predator and prey. In the Holling Type IV functional response, the consumption rate rises slowly as prey population size increases, reaches a maximum rate, and then plateaus while prey population size continues to grow in the Holling Type IV functional response, which is characterized by an S-shaped curve [8, 15].

"Allee effect", is named after ecologist Warder Clyde Allee, who first described it in the 1930s. In a densely populated region, as density increases, the birth rate tends to decrease amid escalating mortality rates. However, an Allee effect is referred to in cases where the birth rate is rising in addition to population growth. A positive association between population density and personal fitness characterizes the Allee effect. For a number of causes, including less mate-seeking, fewer cooperative behaviours, increased susceptibility to predator, or environmental stochasticity, individuals may have decreased fitness at low population densities. These elements may lower fertility rates and slow population growth generally, aggravating the Allee effect [4, 27]. There are observed two types of Allee effect relying on how strongly the per capita growth rate reduces at lower population size, namely strong Allee effect [10, 31–33] and weak Allee effect [27]. For strong (multiplicative) Allee effect, there exists a threshold population level, say, p, with $\frac{1}{N}\frac{dN}{dt} < 0\ (> 0)$ for $N < p$ $(N > p)$ (i.e., per capita growth rate of a population becomes negative at a very low population biomass), where N indicates the population biomass and $\frac{1}{N}\frac{dN}{dt}$ denotes the per capita growth rate. If the growth rate remains positive even after decreasing at a low population size, then the Allee effect is said to be a weak Allee effect, i.e., no threshold of the population size exists in this case. The continuous growth function considering Allee effect is given as $\frac{dN}{dt} = rN\left(1 - \frac{N}{K}\right)\left(\frac{N}{p} - 1\right)$ where r denotes the intrinsic per capita growth rate and K is the carrying capacity of the population. Allee effect expressed by this equation is strong or weak as $p > 0$ or $p < 0$ respectively.

In the present study, we have developed a two-dimensional model that incorporates toxicity in the prey population and strong Allee effect on prey growth. Type IV functional response is also used in the proposed model. We have introduced the model with its parameters in section 2. After that, the positivity and boundedness of the model are shown in section 3. The existence of equilibrium points of the proposed model has been discussed in section 4. After that, in section 5, the detailed study of stability analysis of the equilibrium points are shown. Further, we have described various bifurcation analyses with diagrams in section 6. For a better understanding, we have also performed numerical simulation in section 7 that includes descriptions and analysis of both one and two parametric bifurcations. It also includes the basins of attraction of the proposed system (2.2).

2. Mathematical Model Formulation

Consider the following prey-predator model with Holling type IV functional response and strong Allee effect. In our proposed model the prey population is affected by toxicity due to some toxic substances, and the predator population is also getting affected due to the presence of toxicity in prey. We use the dynamical system below as a basic model representation of prey-predator interaction:

$$\begin{aligned} \frac{dx}{dt} &= rx\left(1 - \frac{x}{K}\right)(x - m_1) - \frac{m_2 xy}{B + x^2} - \xi_1 x^3, \\ \frac{dy}{dt} &= \frac{cm_2 xy}{B + x^2} - h_1 y - \xi_2 y^2. \end{aligned} \tag{2.1}$$

Here, in the above system (2.1): $x(t)$, and $y(t)$ represent the prey biomass and the predator biomass respectively at time t. The intrinsic per capita growth rate of prey in absence of predator is represented as r , K is the carrying capacity of prey in absence of predator. h_1 denotes the natural mortality of predator. Here ξ_1 and ξ_2 are the coefficient of toxicity in the prey population and the predator population respectively and $0 < \xi_2 \leq \xi_1$. m_1 represents the strong Allee threshold value. m_2 is the coefficient of hunting rate of prey by predator. The term c $(0 < c < 1)$ is the conversion factor representing the energetic efficiency in converting consumption of prey into reproduction, and B^{-1} represents the searching rate. We have also listed all parameters and their descriptions, which are used in our proposed model in the table format in Table 1 for easy and quick understanding.

Now, from system (2.1), we get

Table 1: Descriptions of parameters used in this Model

Parameters	Descriptions of Parameters
$x(t)$	Prey biomass at time t
$y(t)$	Predator biomass at time t
r	Per capita growth rate of prey (> 0)
K	Carrying capacity of prey (> 0)
h_1	Natural mortality of predator (> 0)
ξ_1	Coefficient of toxicity of prey population (> 0)
ξ_2	Coefficient of toxicity of predator population (> 0)
m_1	Strong Allee threshold value, where $0 < m_1 << K$
m_2	Coefficient of hunting rate of prey by predator (> 0)
c	Conversion factor ($0 < c < 1$)
B^{-1}	Searching rate (> 0)

$$\begin{aligned} \frac{dx}{dt} &= rx\left(1-\frac{x}{K}\right)(x-m_1) - \frac{m_2xy}{B+x^2} - \xi_1x^3 \equiv F_1(x,y) = xf_1(x,y) \\ \frac{dy}{dt} &= \frac{cm_2xy}{B+x^2} - h_1y - \xi_2y^2 \equiv F_2(x,y) = yf_2(x,y) \end{aligned} \tag{2.2}$$

where

$$f_1(x,y) = r\left(1-\frac{x}{K}\right)(x-m_1) - \frac{m_2y}{B+x^2} - \xi_1x^2$$

and

$$f_2(x,y) = \frac{cm_2x}{B+x^2} - h_1 - \xi_2y$$

3. Postivity and Boundedness

Theorem 3.1. *Every solution of system (2.2) remains positive with initial condition $x(0) > 0$, $y(0) > 0$ for any time $t > 0$.*

Proof: Now from the 1st equation of (2.2)
$\frac{dx}{dt} = xf_1(x,y)$, where $f_1(x,y) = r\left(1-\frac{x}{K}\right)(x-m_1) - \frac{m_2y}{B+x^2} - \xi_1x^2$
$\Rightarrow x(t) = x(0)\exp\left(\int_0^t f_1(x,y)ds\right) > 0$ for $x(0) > 0$.
Now from the 2nd equation of (2.2)
$\frac{dy}{dt} = yf_2(x,y)$, where $f_2(x,y) = \frac{cm_2x}{B+x^2} - h_1 - \xi_2y$
$\Rightarrow y(t) = y(0)\exp\left(\int_0^t f_2(x,y)ds\right) > 0$ for $y(0) > 0$.
Thus $x(t) > 0$ and $y(t) > 0$ whenever $x(0) > 0$, $y(0) > 0$.

Theorem 3.2. *Every solution of system (2.2) with initial condition $x(0) > 0$, $y(0) > 0$ are bounded for any time $t > 0$.*

Proof. First we prove the boundedness for $x(t)$. Here two case arise :
Case I: Assume $x(0) \le K$. Then our claim is $x(t) \le K$ for all $t > 0$. Suppose it is not true then their exist t_1, t_2 with $t_1 < t_2$ such that $x(t_1) = K$ and $x(t) > K$, $\forall\ t \in (t_1, t_2)$.Then for $t \in (t_1, t_2)$,

$$x(t) = x(0) \cdot \exp\left(\int_0^{t_1} f_1(x(s), y(s))ds + \int_{t_1}^{t} f_1(x(s), y(s))ds\right)$$
$$\Rightarrow x(t) = x(0) \cdot \exp\left(\int_0^{t_1} f_1(x(s), y(s))ds\right) \cdot \exp\left(\int_{t_1}^{t} f_1(x(s), y(s))ds\right)$$
$$\Rightarrow x(t) = x(t_1) \cdot \exp\left(\int_{t_1}^{t} f_1(x(s), y(s))ds\right)$$
$$\Rightarrow x(t) = K \cdot \exp\left(\int_{t_1}^{t} f_1(x(s), y(s))ds\right)$$

Now $f_1(x, y) < 0 \ \forall \ t \in (t_1, t_2)$. Then $x(t) < K \ \forall t \in (t_1, t_2)$. Which contradicts our assumption that $x(t) > K \ \forall \ t \in (t_1, t_2)$. Thus we must have $x(t) \leq K \ \forall \ t > 0$.

Case II: Assume $x(0) > K$. Then our claim is that $\limsup_{t\to\infty} x(t) \leq K$. Suppose our claim is false, then there exists $T > 0$, such that $x(t) > K, \ \forall \ t \geq T$. Then $f_1(x, y) < 0, \ \forall \ t \geq T$.

Therefore $x(t) = x(0) \exp\left(\int_0^t f_1(x(s), y(s))ds\right) < x(0)$
Let $\underline{x} = \liminf_{t\to\infty} x(t)$. Then from the 1st equation of (2.2) we get,

$$\frac{dx}{dt} = rx\left(1 - \frac{x}{K}\right)(x - m_1) - \frac{m_2 xy}{B + x^2} - \xi_1 x^3$$
$$\Rightarrow \frac{dx}{dt} \leq rx\left(1 - \frac{x}{K}\right)(x - m_1)$$
$$\Rightarrow \frac{dx}{dt} \leq rx\left(1 - \frac{x}{K}\right)(\underline{x} - m_1) \qquad (as \ \ x(t) > K)$$

Therefore, $\lim_{t\to\infty} x(t) \leq K$. which contradicts our assumption that $x(t) > K \ \forall \ t > 0$.
Hence $\limsup_{t\to\infty} \ x(t) \leq K$. So $x(t)$ is bounded for any time $t > 0$.
Now, we want to prove the boundedness for $y(t)$.
Now,

$$g(x) = \frac{cm_2 x}{B + x^2} \ \ \forall \ x \in [0, K]$$
$$\therefore \ g'(x) = cm_2 \frac{B - x^2}{(B + x^2)^2}$$

Now if, $0 \leq x < \sqrt{B}$ then $g'(x) > 0$ and if, $\sqrt{B} < x < K$ then $g'(x) < 0$. Thus $g(x)$ gives maximum value at $x = \sqrt{B}$.

Now when $\sqrt{B} < K$ then, $\text{Max}\, g(x) = \frac{cm_2\sqrt{B}}{2B} = \frac{cm_2}{2\sqrt{B}}$. For $\sqrt{B} \geq K$ then $\text{Max}\, g(x) = \frac{cm_2 K}{B + K^2}$. Thus from 2nd equation of (2.2),

$$\frac{dy}{dt} \leq y\left[\text{Max}\left\{\frac{cm_2}{2\sqrt{B}}, \frac{cm_2 K}{B + K^2}\right\} - h_1 - \xi_2 y\right]$$
$$\Rightarrow \frac{dy}{dt} \leq y\left[\text{Max}\left\{\frac{cm_2}{2\sqrt{B}}, \frac{cm_2 K}{B + K^2}\right\} - \xi_2 y\right]$$

Let $N = \text{Max}\left\{\frac{cm_2}{2\sqrt{B}}, \frac{cm_2 K}{B + K^2}\right\}$, then $\frac{dy}{dt} \leq \xi_2 y\left(\frac{N}{\xi_2} - y\right) = f_3(y)$.
Therefore, $\limsup_{t\to\infty} y(t) \leq \frac{N}{\xi_2}$. So, $y(t)$ is bounded for any time $t > 0$.

Thus all solutions of the system (2.2) are confined in the region

$$H = \left\{(x, y) : 0 < x(t) \leq K, 0 < y(t) \leq \frac{N}{\xi_2}\right\}$$

Thus clearly every solution of the system (2.2) remains positive with initial condition $x(0) > 0$, $y(0) > 0$ for any time $t > 0$.

4. Equilibrium Point: Existence

Now, we want to find out the equilibrium points for the system (2.2):

$$\frac{dx}{dt} = x\left[r\left(1 - \frac{x}{K}\right)(x - m_1) - \frac{m_2 y}{B + x^2} - \xi_1 x^2\right] = F_1(x, y)$$
$$\frac{dy}{dt} = y\left[\frac{cm_2 x}{B + x^2} - h_1 - \xi_2 y\right] = F_2(x, y)$$

4.1. Axial and Trivial equilibrium

For equilibrium points making $F_1(x, y) = 0$ and $F_2(x, y) = 0$ we see that the system (2.2) has 3 equilibrium points on the non-negative x-axis, which are: $E_0(0, 0)$, $E_{x_1}(x_1, 0)$, $E_{x_2}(x_2, 0)$ where,

$x_1 = \dfrac{r(k + m_1) + \sqrt{r^2(k - m_1)^2 - 4k^2 m_1 r\xi_1}}{2(r + k\xi_1)}$ and $x_2 = \dfrac{r(k + m_1) - \sqrt{r^2(k - m_1)^2 - 4k^2 m_1 r\xi_1}}{2(r + k\xi_1)}$, provided $r^2(k - m_1)^2 > 4k^2 m_1 r\xi_1$. These equilibria are called axial equilibria, among these $E_0(0, 0)$ is known as trivial equilibrium. When $r^2(k - m_1)^2 = 4k^2 m_1 r\xi_1$, the system has two equilibrium points on non-negative x-axis, which are: $E_0(0, 0)$, $E_{x^*}(x^*, 0)$, where $x^* = \dfrac{r(K + m_1)}{2(r + K\xi_1)}$.

4.2. Interior equilibrium

Now, the interior equilibrium point of the system (2.2) is found out by solving two non-trivial nullclines, which are

$$f_1(x, y) = 0 \Rightarrow y = \frac{r}{m_2}(B + x^2)\left(1 - \frac{x}{K}\right)(x - m_1) - \frac{\xi_1}{m_2}x^2(B + x^2) \tag{4.1}$$

$$f_2(x, y) = 0 \Rightarrow y = \frac{1}{\xi_2}\left(\frac{cm_2 x}{B + x^2} - h_1\right) \tag{4.2}$$

Now, (4.2) and (4.1) lead to

$$\phi(x) = 0 \tag{4.3}$$

where $\phi(x) = a_0x^6 - a_1x^5 + a_2x^4 - a_3x^3 + a_4x^2 - a_5x + a_6$
Here,

$$\begin{aligned}
a_0 &= \xi_2(r + K\xi_1)\\
a_1 &= r\xi_2(m_1 + K)\\
a_2 &= \xi_2(rm_1K + 2Br + 2BK\xi_1)\\
a_3 &= 2Br\xi_2(m_1 + K)\\
a_4 &= \xi_2(B^2r + B^2\xi_1K + 2BKrm_1) - h_1m_2K\\
a_5 &= B^2\xi_2r(m_1 + K) - cm_2^2K\\
a_6 &= B^2Krm_1\xi_2 - BKh_1m_2
\end{aligned}$$

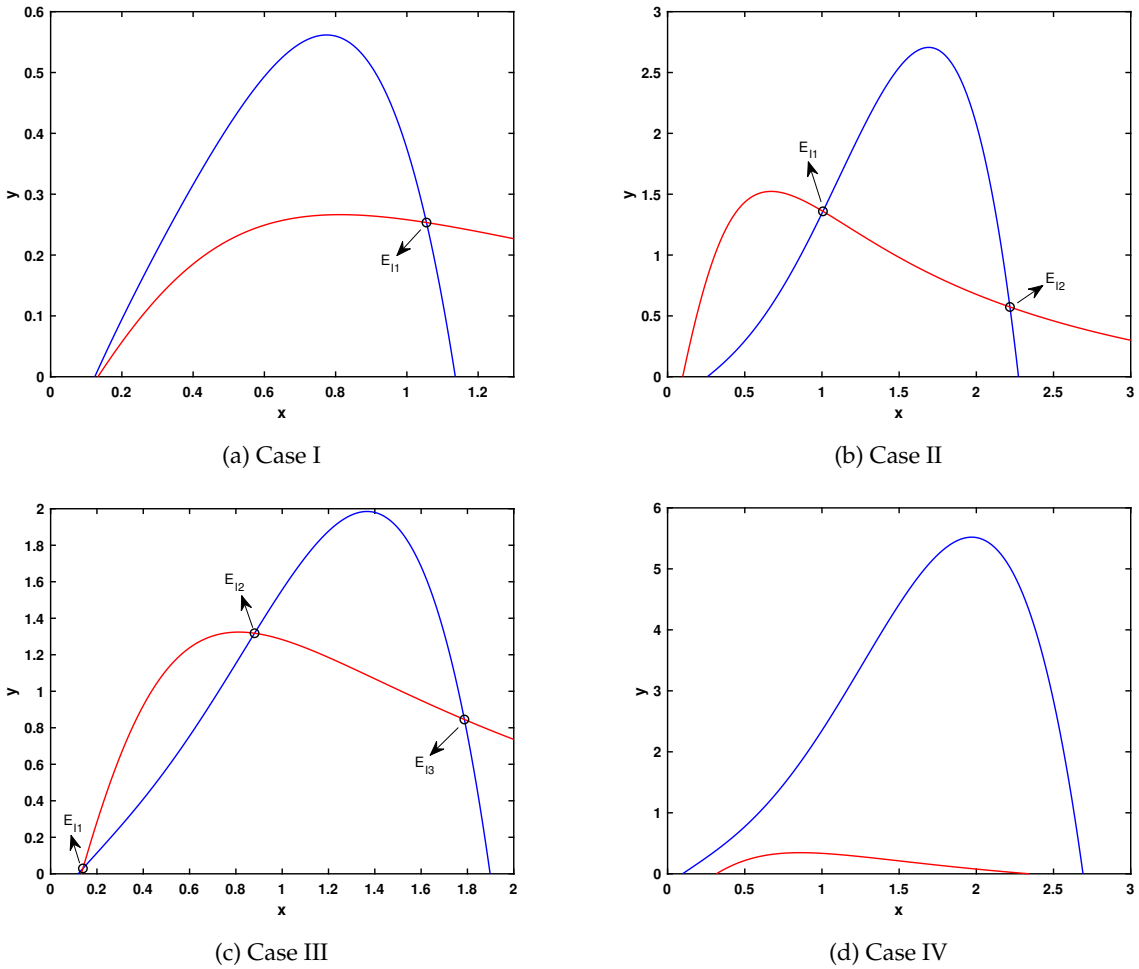

(a) Case I (b) Case II

(c) Case III (d) Case IV

Figure 1: Variation in the number of interior equilibrium point for a suitable choice of parameters. Here blue and red curve denotes the non-trivial x and y nullcline respectively.

Now, $a_0, a_1, a_2, a_3 > 0$. When $a_6 < 0$, by Descartes's rule of sign [2] we can say the equation $\phi(x) = 0$ has at least one positive solution, Let it be x_3, then from equation (4.3), we get

$$y = \frac{1}{\xi_2}\left(\frac{cm_2x_3}{B + x_3^2} - h_1\right) = y_3 \ \ (say) \ \ provided \ \ cm_2x_3 > h_1(B + x_3^2)$$

Thus $E_I(x_3, y_3)$ is an interior equilibrium of system (2.2)
For a suitable choice of parameters, there are some variations in the existence of the interior equilibrium of the system (2.2). Numerically, we obtain some cases, which are given below:
Case I: If we set the parameter values as $r = 1.73, K = 4, m_1 = 0.115, B = 0.66, c = 0.733, h_1 = 0.107, \xi_1 = 0.98, \xi_2 = 0.86, m_2 = 0.745$, the non-trivial prey nullcline and non-trivial predator nullcline intersect only at one point, which is an interior equilibrium of the system (2.2) and it is denoted by $E_{I1}(x_3', y_3')$. The corresponding diagram is shown in Fig.1a.

Case II: Next if we set the parameter values as $r = 1.73, K = 4, m_1 = 0.246, B = 0.45, c = 0.68, h_1 = 0.107, \xi_1 = 0.293, \xi_2 = 0.176, m_2 = 0.74$, the non-trivial prey and predator nullclines intersect two times,

which are the respective interior equilibrium points of the system and they are denoted by $E_{I1}(x_3^{'}, y_3^{'})$ and $E_{I2}(x_3^{''}, y_3^{''})$. The corresponding diagram is shown in Fig.1b.

Case III: If we set the parameter values as $r = 1.73, K = 4, m_1 = 0.115, B = 0.66, c = 0.733, h_1 = 0.107, \xi_1 = 0.45, \xi_2 = 0.173, m_2 = 0.745$, the non-trivial prey and predator nullclines intersect three times, which are the corresponding interior equilibrium points of the system and they are denoted by $E_{I1}(x_3^{'}, y_3^{'})$, $E_{I2}(x_3^{''}, y_3^{''})$ and $E_{I3}(x_3^{'''}, y_3^{'''})$. The corresponding diagram is shown in Fig.1c.

Case IV: Now if we set the parameter values as $r = 1.72, K = 4.26, m_1 = 0.096, B = 0.74, c = 0.41, h_1 = 0.11, \xi_1 = 0.227, \xi_2 = 0.173, m_2 = 0.713$, the non-trivial prey and predator nullclines do not intersect to each other. The corresponding diagram is shown in Fig.1d.

5. Stability Analysis

Now the Jacobian matrix of the system (2.2) at the equilibrium point $E(x, y)$ is given by

$$J(x,y) = \begin{bmatrix} \frac{\partial F_1}{\partial x} & \frac{\partial F_1}{\partial y} \\ \frac{\partial F_2}{\partial x} & \frac{\partial F_2}{\partial y} \end{bmatrix}$$

$$= \begin{bmatrix} r(1-\frac{x}{K})(x-m_1) + rx(1-\frac{x}{K}) - \frac{rx}{K}(x-m_1) - \frac{m_2 y(B-x^2)}{(B+x^2)^2} - 3\xi_1 x^2 & -\frac{m_2 x}{B+x^2} \\ \frac{cm_2 y(B-x^2)}{(B+x^2)^2} & \frac{cm_2 x}{B+x^2} - h_1 - 2\xi_2 y \end{bmatrix}$$

Theorem 5.1. *The trivial equilibrium point $E_0(0,0)$ is always locally asymptotically stable.*

Proof. Now the Jacobian matrix of the system (2.2) at the trivial equilibrium point $E_0(0,0)$ is given by,

$$J(E_0) = \begin{bmatrix} -rm_1 & 0 \\ 0 & -h_1 \end{bmatrix} = A$$

The characteristic equation for the matrix A is given by,

$$|A - \lambda I| = 0 \Rightarrow \lambda = -h_1, -rm_1$$

Since $h_1, r, m_1 > 0$, both eigenvalues are always negative. Thus the trivial equilibrium point $E_0(0.0)$ is always locally asymptotically stable.

Theorem 5.2. *The axial equilibrium point $E_{x_1}(x_1, 0)$ which is predator-free is (i) stable node if $\frac{cm_2x_1}{B+x_1^2} < h_1$ and (ii) unstable saddle if $\frac{cm_2x_1}{B+x_1^2} > h_1$*

Proof. The Jacobian matrix of system (2.2) at the equilibrium point $E_{x_1}(x_1, 0)$ is given by,

$$J(x_1,0) = \begin{bmatrix} r\left(1-\frac{x_1}{K}\right)(x_1-m_1) + rx_1\left(1-\frac{x_1}{K}\right) - \frac{rx_1}{K}(x_1-m_1) - 3\xi_1 x_1^2 & -\frac{m_2 x_1}{B+x_1^2} \\ 0 & \frac{cm_2x_1}{B+x_1^2} - h_1 \end{bmatrix}.$$

Here, we use $r\left(1-\frac{x_1}{K}\right)(x_1-m_1) = \xi_1 x_1^2$; as nontrivial nullcline for $\frac{dx}{dt} = 0$ satisfy by $E_{x_1}(x_1, 0)$.

$$J(x_1,0)=\begin{bmatrix} -\left(\frac{2r}{K}+2\xi_1\right)x_1^2+rx_1\left(1+\frac{m_1}{K}\right) & -\frac{m_2x_1}{B+x_1^2} \\ 0 & \frac{cm_2x_1}{B+x_1^2}-h_1 \end{bmatrix}=A_1$$

Now, the characteristic equation for the matrix A_1 is given by,

$$|A_1-\lambda I|=0$$

$$\Rightarrow \lambda=-\left(\frac{2r}{K}+2\xi_1\right)x_1^2+rx_1\left(1+\frac{m_1}{K}\right),\frac{cm_2x_1}{B+x_1^2}-h_1.$$

Here, $rx_1\left(1+\frac{m_1}{K}\right)<\left(\frac{2r}{K}+2\xi_1\right)x_1^2$

$\Rightarrow x_1>\frac{r(K+m_1)}{2(r+K\xi_1)}$; where $x_1=\frac{r(K+m_1)}{2(r+K\xi_1)}+\frac{\sqrt{r^2(K-m_1)^2-4K^2m_1r\xi_1}}{2(r+K\xi_1)}$.

But on the other hand, if $rx_1\left(1+\frac{m_1}{K}\right)>\left(\frac{2r}{K}+2\xi_1\right)x_1^2$, $x_1<\frac{r(K+m_1)}{2(r+K\xi_1)}$, which is a contradiction.

Case I: When $rx_1\left(1+\frac{m_1}{K}\right)<\left(\frac{2r}{K}+2\xi_1\right)x_1^2$ and $\frac{cm_2x_1}{B+x_1^2}<h_1$, both eigenvalues are negative. So $E_{x_1}(x_1,0)$ is stable node.

Case II: When $rx_1\left(1+\frac{m_1}{K}\right)<\left(\frac{2r}{K}+2\xi_1\right)x_1^2$ and $\frac{cm_2x_1}{B+x_1^2}>h_1$, one eigenvalue is positive and another is negative. So, $E_{x_1}(x_1,0)$ is an unstable Saddle point.

Theorem 5.3. *The axial equilibrium point $E_{x_2}(x_2,0)$ which is predator-free is (i) unstable saddle if $\frac{cm_2x_2}{B+x_2^2}<h_1$ and (ii) unstable node if $\frac{cm_2x_2}{B+x_2^2}>h_1$*

Proof. Now the Jacobian matrix of the system (2.2) at the equilibrium point $E_{x_2}(x_2,0)$ is given by

$$J(x_2,0)=\begin{bmatrix} r\left(1-\frac{x_2}{K}\right)(x_2-m_1)+rx_2\left(1-\frac{x_2}{K}\right)-\frac{rx_2}{K}(x_2-m_1)-3\xi_1x_2^2 & -\frac{m_2x_2}{B+x_2^2} \\ 0 & \frac{cm_2x_2}{B+x_2^2}-h_1 \end{bmatrix}.$$

Here, we use $r\left(1-\frac{x_2}{K}\right)(x_2-m_1)=\xi_1x_2^2$, as nontrivial nullcline for $\frac{dx}{dt}=0$ satisfy by $E_{x_2}(x_2,0)$.

$$J(x_2,0)=\begin{bmatrix} -\left(\frac{2r}{K}+2\xi_1\right)x_2^2+rx_2\left(1+\frac{m_1}{K}\right) & -\frac{m_2x_2}{B+x_2^2} \\ 0 & \frac{cm_2x_2}{B+x_2^2}-h_1 \end{bmatrix}=A_2.$$

Now, the characteristic equation for the matrix A_2 is given by,

$$|A_2-\lambda I|=0$$

$$\Rightarrow \lambda=-\left(\frac{2r}{K}+2\xi_1\right)x_2^2+rx_2\left(1+\frac{m_1}{K}\right),\frac{cm_2x_2}{B+x_2^2}-h_1.$$

Here, $rx_2\left(1+\frac{m_1}{K}\right)>\left(\frac{2r}{K}+2\xi_1\right)x_2^2$

$\Rightarrow x_2<\frac{r(K+m_1)}{2(r+K\xi_1)}$; where $x_2=\frac{r(K+m_1)}{2(r+K\xi_1)}-\frac{\sqrt{r^2(K-m_1)^2-4K^2m_1r\xi_1}}{2(r+K\xi_1)}$

But on the other hand, if $rx_2\left(1+\frac{m_1}{K}\right) < \left(\frac{2r}{K}+2\xi_1\right)x_2^2$, then $x_2 > \frac{r(K+m_1)}{2(r+K\xi_1)}$, which is a contradiction.

Case I: When $rx_2\left(1+\frac{m_1}{K}\right) > \left(\frac{2r}{K}+2\xi_1\right)x_2^2$ and $\frac{cm_2x_2}{B+x_2^2} < h_1$, one eigenvalue is positive and another eigenvalue is negative. So, $E_{x_2}(x_2,0)$ is an unstable saddle point.

Case II: When $rx_2\left(1+\frac{m_1}{K}\right) > \left(\frac{2r}{K}+2\xi_1\right)x_2^2$ and $\frac{cm_2x_2}{B+x_2^2} > h_1$, both eigenvalues are positive. So, $E_{x_2}(x_2,0)$ is unstable node.

Theorem 5.4. *The interior equilibrium point $E_I(x_3,y_3)$ in which both species survive, is*
(i) stable node if $\alpha<0,\beta>0,\alpha^2-4\beta\geq 0$
(ii) unstable node if $\alpha>0,\beta>0,\alpha^2-4\beta\geq 0$
(iii) stable spiral if $\alpha<0,\alpha^2-4\beta<0$
(iv) unstable spiral if $\alpha>0,\alpha^2-4\beta<0$
(v) unstable saddle if $\beta<0,\alpha^2-4\beta\geq 0$
(vi) stable centre if $\alpha=0,\beta>0$
where $\alpha=Tr(J(x_3,y_3))$ and $\beta=det(J(x_3,y_3))$.

Proof. Now, the Jacobian matrix of system (2.2) at interior equilibrium point $E_I(x_3,y_3)$ is given by

$$J(x_3,y_3)=\begin{bmatrix} x\frac{\partial f_1}{\partial x} & x\frac{\partial f_1}{\partial y} \\ y\frac{\partial f_2}{\partial x} & y\frac{\partial f_2}{\partial y}\end{bmatrix}_{(x_3,y_3)}$$

$$=\begin{bmatrix} J_{11} & J_{12} \\ J_{21} & J_{22}\end{bmatrix}=A_3$$

where,

$$\begin{aligned} J_{11} &= rx_3(1-\frac{x_3}{K})-\frac{rx_3}{K}(x_3-m_1)+\frac{2m_2y_3x_3^2}{(B+x_3^2)^2}-2\xi_1x_3^2 \\ J_{12} &= -\frac{m_2x_3}{(B+x_3^2)} \\ J_{21} &= \frac{cm_2y_3(B-x_3^2)}{(B+x_3^2)^2} \\ J_{22} &= -\xi_2y_3 \end{aligned}$$

Now, the characteristic equation for the matrix A_3 is given by

$$|A_3-\lambda I|=0\Rightarrow \lambda^2-\alpha\lambda+\beta=0$$

$$\Rightarrow \lambda=\lambda_1,\lambda_2 \text{ where } \lambda_1=\frac{\alpha+\sqrt{\alpha^2-4\beta}}{2},\lambda_2=\frac{\alpha-\sqrt{\alpha^2-4\beta}}{2}.$$

Here, $\beta=det(J(x_3,y_3))=(J_{11}J_{22}-J_{21}J_{12})$

$$=-r\xi_2x_3y_3(1-\frac{x_3}{K})+\frac{r\xi_2x_3y_3}{K}(x_3-m_1)-\frac{2m_2\xi_2y_3^2x_3^2}{(B+x_3^2)^2}+2\xi_1\xi_2x_3^2y_3+cm_2^2x_3y_3\frac{(B-x_3^2)}{(B+x_3^2)^3},$$

$\alpha=Tr(J(x_3,y_3))=J_{11}+J_{22}$

$$= rx_3(1-\frac{x_3}{K}) - \frac{rx_3}{K}(x_3-m_1) + \frac{2m_2y_3x_3^2}{(B+x_3^2)^2} - 2\xi_1x_3^2 - \xi_2y_3$$

Case-I: If $\alpha < 0, \beta > 0, \alpha^2 - 4\beta \geq 0$, both eigenvalues λ_1 and λ_2 are negative. So (x_3, y_3) is a stable node equilibrium point.
Case-II: If $\alpha > 0, \beta > 0, \alpha^2 - 4\beta \geq 0$, both eigenvalues λ_1 and λ_2 are positive. So (x_3, y_3) is the unstable node equilibrium point.
Case-III: If $\alpha < 0, \alpha^2 - 4\beta < 0$, both eigenvalues λ_1 and λ_2 are imaginary with negative real part. So (x_3, y_3) is a stable spiral equilibrium point.
Case-IV: If $\alpha > 0, \alpha^2 - 4\beta < 0$, both eigenvalues λ_1 and λ_2 are imaginary with positive real part. So (x_3, y_3) is an unstable spiral equilibrium point.
Case-V: If $\beta < 0, \alpha^2 - 4\beta \geq 0$, among the eigenvalues λ_1 and λ_2 , one is positive and another is negative. So (x_3, y_3) is an unstable saddle equilibrium point.
Case-VI: If $\alpha = 0, \beta > 0$, both eigenvalues λ_1 and λ_2 are purely imaginary. So (x_3, y_3) is a stable centre equilibrium point.

6. Bifurcation Analysis

In this particular section, our focus is directed towards an exhaustive exploration of all possible local bifurcations associated with system (2.2). Here we specifically explore transcritical bifurcation, saddle-node bifurcation, and Hopf bifurcation, which are of codimension 1, as well as cusp bifurcation and Bogdanov-Takens bifurcation, which are of codimension 2. Our inevstigation centers around how these bifurcations contribute to alterations in the stability of the equilibrium point.

6.1. Transcritical Bifurcation

The fundamental process by which an equilibrium point of the system exchanges its stability with another equilibrium point for the variation of a parameter is referred as transcritical bifurcation. Here we show that system (2.2) experiences a transcritical bifurcation for the bifurcating parameter h_1, which leads to an exchange of stability between the predator-free equilibrium point $E_{x_1}(x_1, 0)$ and interior equilibrium point $E_I(x_3, y_3)$.

Theorem 6.1. *System (2.2) undergoes a transcritical bifurcation, leading to a stability swaps between $E_{x_1}(x_1, 0)$ and $E_I(x_3, y_3)$, as h_1 is varied through the bifurcation threshold $h_1 = h_1^{(TC)} = \dfrac{cm_2x_1}{B+x_1^2}$.*

Proof: For $h_1 = h_1^{(TC)}$, the evaluation of the Jacobian matrix at $E_{x_1}(x_1, 0)$ is

$$J(E_{x_1})\big|_{h_1=h_1^{(TC)}} = \begin{bmatrix} rx_1\left(1+\frac{m_1}{K}\right) - \left(\frac{2r}{K}+2\xi_1\right)x_1^2 & -\frac{m_2x_1}{B+x_1^2} \\ 0 & 0 \end{bmatrix} = B_1 \quad \text{(say)}$$

Since $det(B_1) = 0$, one of the eigenvalues of B_1 is 0. So 0 is also an eigenvalue of B_1^T. Now the eigenvectors of B_1 and B_1^T corresponding to eigenvalue 0 are given by $W = \begin{bmatrix} 1 \\ \frac{\left(B+x_1^2\right)}{Km_2}\left\{r\left(K+m_1\right) - 2\left(K\xi_1+r\right)x_1\right\} \end{bmatrix}$ and $Z = \begin{bmatrix} 0 \\ 1 \end{bmatrix}$, respectively. Now we apply Sotomayor's theorem [17] to prove the existence of a transcritical

bifurcation at $h_1 = h_1^{(TC)} = \dfrac{cm_2x_1}{B + {x_1}^2}$. Now,

$$\begin{aligned}
Z^T\left[F_{h_1}\left(E_{x_1}, h_1^{(TC)}\right)\right] &= 0\\
Z^T\left[DF_{h_1}\left(E_{x_1}, h_1^{(TC)}\right)W\right] &= \frac{2\left(B+x_1^2\right)(r+K\xi_1)}{Km_2}\left[x_1 - \frac{r\,(K+m_1)}{2\,(r+K\xi_1)}\right] \neq 0;\ \text{since } \mathrm{x_1} > \frac{\mathrm{r(K+m_1)}}{\mathrm{2(r+K\xi_1)}}\\
Z^T\left[D^2F\left(E_{x_1}, h_1^{(TC)}\right)(W,W)\right] &= \frac{4c\left(B-x_1^2\right)}{K\left(B+x_1^2\right)}(r+K\xi_1)\left[\frac{r\,(K+m_1)}{2\,(r+K\xi_1)} - x_1\right] -\\
&\quad \frac{8\xi_2\left(B+x_1^2\right)^2}{K^2m_2^2}(r+K\xi_1)^2\left[\frac{r\,(K+m_1)}{2\,(r+K\xi_1)} - x_1\right]^2;\ \text{where } \mathrm{x_1} > \frac{\mathrm{r(K+m_1)}}{\mathrm{2(r+K\xi_1)}}
\end{aligned}$$

Here $F \equiv \begin{pmatrix} F_1 \\ F_2 \end{pmatrix}$ and each of F_1, F_2 are defined in (2.2). Now, $Z^T\left[D^2F\left(E_{x_1}, h_1^{(TC)}\right)(W,W)\right] < 0$, provided

(*i*) $B \geq x_1^2$, or

(*ii*) $B < x_1^2,\ c < \dfrac{2\xi_2\left(B+x_1^2\right)^3(r+K\xi_1)}{Km_2^2\left(x_1^2-B\right)}\left[x_1 - \dfrac{r\,(K+m_1)}{2\,(r+K\xi_1)}\right]$

and $Z^T\left[D^2F\left(E_{x_1}, h_1^{(TC)}\right)(W,W)\right] > 0$, provided $B < x_1^2,\ \ c > \frac{2\xi_2\left(B+x_1^2\right)^3(r+K\xi_1)}{Km_2^2\left(x_1^2-B\right)}\left[x_1 - \frac{r(K+m_1)}{2(r+K\xi_1)}\right]$. So in both cases, $Z^T\left[D^2F\left(E_{x_1}, h_1^{(TC)}\right)(W,W)\right] \neq 0$. Therefore, the transversality conditions for transcritical bifurcation are satisfied and the system experiences a transcritical bifurcation around $E_{x_1}(x_1, 0)$ at the bifurcation threshold $h_1 = h_1^{(TC)} = \dfrac{cm_2x_1}{B+x_1^2}$.

6.2. Saddle-Node Bifurcation

A saddle-node bifurcation occurs when, due to the variation of a parameter, two equilibrium points within the system approach each other, collide, and then disappear through mutual annihilation. Here we take ξ_2 as a bifurcation parameter. Earlier, it was demonstrated that the system may possesses multiple coexistence equilibrium points. When two such coexistence equilibrium points coincide, a saddle-node bifurcation emerges. Through nullcline analysis, it becomes evident that this saddle-node bifurcation occurs precisely when the prey and predator nullclines make tangential contact. A numerical demonstration is given in Fig.2, where the non-trivial prey and predator nullclines touches each other at $E_{I1}(x', y')$ for $\xi_2 = \xi_2^{(SN_1)} = 0.4429$ and at $E_{I2}(x'', y'')$ for $\xi_2 = \xi_2^{(SN_2)} = 0.0919$. The values of other parameters for these two figures are same i.e., $r = 1.73, K = 4, m_1 = 0.115, B = 0.66, c = 0.733, h_1 = 0.107, \xi_1 = 0.45, m_2 = 0.745$.
Now we prove a theorem, demonstarting that the system experiences a saddle-node bifurcation with respect to bifurcation parameter ξ_2.

Theorem 6.2. *System (2.2) undergoes a saddle-node bifurcation with respect to the bifurcation parameter ξ_2.*

Proof: Let x' represent the double root of $\phi(x) = 0$ occurring at $\xi_2 = \xi_2^{(SN_1)}$, where $\phi(x) = a_0x^6 - a_1x^5 + a_2x^4 - a_3x^3 + a_4x^2 - a_5x + a_6$. The coefficients $a_0, a_1, a_2, a_3, a_4, a_5$ and a_6 are defined in section 4.2. In this case, two non trivial nullclines $f_1(x, y) = 0$ and $f_2(x, y) = 0$ make a tangential contact at $E_{I1}(x', y')$. Then $\left.\dfrac{dy^{(f_1)}}{dx}\right|_{E_{I1}} = \left.\dfrac{dy^{(f_2)}}{dx}\right|_{E_{I1}}$. The Jacobian matrix $J(E_{I1})$ at $\xi_2 = \xi_2^{(SN_1)}$ is given by

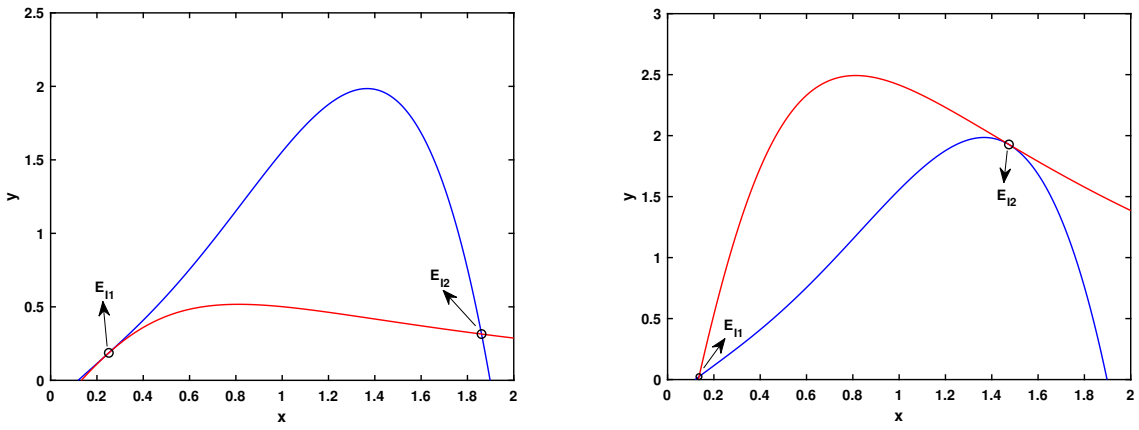

(a) $\xi_2 = 0.4429$ (b) $\xi_2 = 0.0919$

Figure 2: The positions of non-trivial prey and predator nullclines corresponding to the occurrence of saddle–node bifurcations. Here the blue curve and red curve denote the non-trivial prey and predator nullcline respectively.

$$J(E_{I1}) = \left[\begin{array}{cc} x\frac{\partial f_1}{\partial x} & x\frac{\partial f_1}{\partial y} \\ y\frac{\partial f_2}{\partial x} & y\frac{\partial f_2}{\partial y} \end{array}\right]_{E_{I1},\xi_2^{(SN_1)}}$$

$$= \left[\begin{array}{cc} rx\left(1-\frac{x}{K}\right) - \frac{rx}{K}(x-m_1) + \frac{2m_2yx^2}{(B+x^2)^2} - 2\xi_1x^2 & -\frac{m_2x}{(B+x^2)} \\ cm_2y\frac{\left(B-x^2\right)}{(B+x^2)^2} & -\xi_2y \end{array}\right]_{E_{I1},\xi_2^{(SN_1)}}$$

Now,

$$det(J(E_{I1})) = \left[xy\left(\frac{\partial f_1}{\partial x}\frac{\partial f_2}{\partial y} - \frac{\partial f_1}{\partial y}\frac{\partial f_2}{\partial x}\right)\right]_{E_{I1},\xi_2^{(SN_1)}} = \left[xy\frac{\partial f_1}{\partial y}\frac{\partial f_2}{\partial y}\left(\frac{dy^{(f_2)}}{dx} - \frac{dy^{(f_1)}}{dx}\right)\right]_{E_{I1},\xi_2^{(SN_1)}} = 0.$$

Let, $J(E_{I1}) = B_2$ and $J^T(E_{I1}) = B_2^T$. Since $det(J(E_{I1})) = 0$, 0 is an eigenvalue of B_2 and B_2^T. Now the eigenvectors of B_2 and B_2^T corresponding to this zero eigenvalue are given by $W = \left[\begin{array}{c} w_1 \\ w_2 \end{array}\right]_{E_{I1},\xi_2^{(SN_1)}}$ and $Z = \left[\begin{array}{c} z_1 \\ z_2 \end{array}\right]_{E_{I1},\xi_2^{(SN_1)}}$ respectively, where $w_1 = 1$, $w_2 = \frac{cm_2(B-x^2)}{\xi_2(B+x^2)^2}$, $z_1 = -\frac{\xi_2y(B+x^2)}{m_2x}$ and $z_2 = 1$. Using the Sotomayor's theorem [17] at $\xi_2 = \xi_2^{(SN_1)}$, we have

Now, $Z^T F_{\xi_2}(E_{I1}, \xi_2^{(SN_1)}) = -(y')^2 \neq 0$

$$Z^T\left[D^2F(E_{I1}, \xi_2^{(SN_1)})(W,W)\right] =$$

$$\left[\left(-\frac{\xi_2y(B+x^2)}{m_2x}\right)\cdot\left({w_1}^2\frac{\partial^2F_1}{\partial x^2} + 2w_1w_2\frac{\partial^2F_1}{\partial x\partial y} + {w_2}^2\frac{\partial^2F_1}{\partial y^2}\right) + \left({w_1}^2\frac{\partial^2F_2}{\partial x^2} + 2w_1w_2\frac{\partial^2F_2}{\partial x\partial y} + {w_2}^2\frac{\partial^2F_2}{\partial y^2}\right)\right]_{E_{I1},\xi_2^{(SN_1)}}$$

$$= \left[\frac{\xi_2\left\{y\left(B+x^2\right)^3(6rx+6\xi_1 Kx-2rK-2rm_1)-2m_2xy^2\left(3B-x^2\right)\right\}}{Km_2x\left(B+x^2\right)^2} + 2cm_2y\frac{\left(2x^4+B^2-5Bx^2\right)}{x\left(B+x^2\right)^3} \right]_{E_{I1},\xi_2^{(SN_1)}} \neq 0,$$

provided $c \neq \left[\frac{\xi_2\left[y\left(B+x^2\right)^3(6rx+6\xi_1 Kx-2rK-2rm_1)-2Km_2xy^2(3B-x^2)\right](B+x^2)}{2m_2^2y\left(5Bx^2-B^2-2x^4\right)} \right]_{E_{I1},\xi_2^{(SN_1)}}$

Here $F \equiv \begin{pmatrix} F_1 \\ F_2 \end{pmatrix}$ and each of F_1, F_2 are defined in (2.2). Therefore, the transversality conditions for saddle-node bifurcation are satisfied and the system undergoes a saddle-node bifurcation at $\xi_2 = \xi_2^{(SN_1)}$. In similar way, it can be easily demonstrated that another saddle-node bifurcation occur at $\xi_2 = \xi_2^{(SN_2)}$.

Theorem 6.3. *For the bifurcating parameter h_1, system (2.2) undergoes a saddle-node bifurcations at $h_1 = h_1^{(SN)}$.*

Proof. The proof is similar as Theorem 6.2 and is omitted.

Theorem 6.4. *For the bifurcating parameter ξ_1, system (2.2) undergoes two saddle-node bifurcations:*
(i) one is for interior equilibrium state at $\xi_1 = \xi_1^{(SN_1)}$ and
(ii) other one is for axial equilibrium state at $\xi_1 = \xi_1^{(SN_2)}$.

Proof. (i) The proof is similar to Theorem 6.2 and is omitted.
(ii) For $\xi_1 = \xi_1^{(SN_2)}$, the evaluation of the Jacobian matrix at axial equilibrium point $E_{x^*}(x^*, 0)$, where $x^* = \frac{r(k+m_1)}{2(r+k\xi_1)}$ is given by

$$J(E_{x^*})|_{\xi_1=\xi_1^{(SN_2)}} = \begin{bmatrix} 0 & -\frac{m_2x^*}{(B+x^{*2})} \\ 0 & \frac{cm_2x^*}{B+x^{*2}} - h_1 \end{bmatrix} = G.$$

Since $det(G) = 0$, 0 is an eigenvalue of G and G^T. The eigenvectors of G and G^T corresponding to zero eigenvalue are given by $W = \begin{bmatrix} 1 \\ 0 \end{bmatrix}$ and $Z = \begin{bmatrix} 1 \\ \frac{m_2x^*}{cm_2x^* - h_1(B+x^{*2})} \end{bmatrix}$ respectively, provided $cm_2x^* \neq h_1(B+x^{*2})$. Now we apply Sotomayor's theorem [17] to prove that the system (2.2) undergoes a saddle-node bifurcation at $\xi_1 = \xi_1^{(SN_2)}$. Now,

$$\begin{aligned} Z^T F_{\xi_1}(E_{x^*}, \xi_1^{(SN_2)}) &= -x^{*3} \neq 0 \\ Z^T\left[D^2F(E_{x^*}, \xi_1^{(SN_2)})(W,W)\right] &= -\frac{r(K+m_1)}{K} \neq 0 \end{aligned}$$

Here, $F = \begin{pmatrix} F_1 \\ F_2 \end{pmatrix}$ and each of F_1, F_2 are defined in (2.2). Therefore, the transversality conditions for saddle-node bifurcation are satisfied and the system experiences a saddle-node bifurcation at $\xi_1 = \xi_1^{(SN_2)}$ around $E_{x^*}(x^*, 0)$.

Theorem 6.5. *For the bifurcating parameter m_1, system (2.2) undergoes two saddle-node bifurcations:*
(i) one is for interior equilibrium state at $m_1 = m_1^{(SN_1)}$ and
(ii) other one is for axial equilibrium state at $m_1 = m_1^{(SN_2)}$.

Proof. The proof is similar to Theorem 6.4 and is omitted.

6.3. Hopf Bifurcation

If we take ξ_1 as a varying parameter, the characteristic equation of system (2.2) for the Jacobian matrix $J(E_I(x_3, y_3))$ can be written as

$$\lambda^2 - T(\xi_1)\lambda + D(\xi_1) = 0 \tag{6.1}$$

where $T(\xi_1)$ and $D(\xi_1)$ are the trace and determinant of the Jacobian matrix for the interior equilibrium point $E_I(x_3, y_3)$, explicitly defined in the proof of Theorem 5.4. Here one can observe a change in the sign of the real part of λ from negative to positive results in a shift of stability for the interior equilibrium point $E_I(x_3, y_3)$, effectively transitioning it from a stable state to an unstable one. This change occurs through a Hopf bifurcation when the characteristic equation (6.1) contains pair of purely imaginary roots. Suppose those purely imaginary roots occur at $\xi_1 = \xi_1^{(H)}$. Then $T(\xi_1^{(H)}) = 0$, $D(\xi_1^{(H)}) > 0$. In the following theorem, we establish the presence of a Hopf bifurcation within the system occurring at $\xi_1 = \xi_1^{(H)}$.

Theorem 6.6. *For the bifurcation parameter ξ_1, system (2.2) undergoes a Hopf bifurcation around the interior equilibrium state $E_I(x_3, y_3)$ at $\xi_1 = \xi_1^{(H)}$, provided $T(\xi_1^{(H)}) = 0$, $D(\xi^{(H)}) > 0$ and* $\left[\frac{dT}{d\xi_1}\right]_{\xi_1=\xi_1^{(H)}} \neq 0$.

Proof. At $\xi_1 = \xi_1^{(H)}$, $T(\xi_1^{(H)}) = 0$ and $D(\xi_1^{(H)}) > 0$. The characteristic equation (6.1) has purely imaginary roots, which are given by $\lambda_1 = i\sqrt{D(\xi_1^{(H)})}$ and $\lambda_2 = -i\sqrt{D(\xi_1^{(H)})}$. Therefore, in any open neighborhood of $\xi_1^{(H)}$, the roots of the characteristic equation (6.1) have the form $\lambda_1 = q_1(\xi_1) + iq_2(\xi_1)$ and $\lambda_2 = q_1(\xi_1) - iq_2(\xi_1)$, where $q_1(\xi_1)$ and $q_2(\xi_1)$ are the real valued functions of ξ_1. Using the Hopf-Bifurcation Theorem [16], we can say that the system switches its stability through a Hopf bifurcation provided the following transversality condition

$$\left[\frac{d}{d\xi_1}(Re(\lambda_i(\xi_1)))\right]_{\xi_1=\xi_1^{(H)}} = \left[\frac{dq_1(\xi_1)}{d\xi_1}\right]_{\xi_1=\xi_1^{(H)}} \neq 0$$

is satisfied. Putting $\lambda(\xi_1) = q_1(\xi_1) + iq_2(\xi_1)$ in (6.1), we get

$$(q_1(\xi_1) + iq_2(\xi_1))^2 - T(\xi_1)(q_1(\xi_1) + iq_2(\xi_1)) + D(\xi_1) = 0.$$

Now differentiating both sides w.r.t ξ_1, we get

$$2\left(q_1\left(\xi_1\right) + iq_2\left(\xi_1\right)\right)\left(\dot{q}_1\left(\xi_1\right) + i\dot{q}_2\left(\xi_1\right)\right) - T\left(\xi_1\right)\left(\dot{q}_1\left(\xi_1\right) + i\dot{q}_2\left(\xi_1\right)\right) - \dot{T}\left(\xi_1\right)\left(q_1\left(\xi_1\right) + iq_2(\xi_1)\right) + \dot{D}\left(\xi_1\right) = 0$$

Now comparing the real and imaginary parts on both sides, we get

$$\left(2q_1 - T\right)\dot{q}_1 - 2\dot{q}_2 q_2 - \dot{T}q_1 + \dot{D} = 0 \Rightarrow \dot{q}_1 Y_1 - \dot{q}_2 Y_2 + Y_3 = 0 \tag{6.2}$$

$$\left(2q_2\right)\dot{q}_1 + \left(2q_1 - T\right)\dot{q}_2 - \dot{T}q_2 = 0 \Rightarrow \dot{q}_1 Y_2 + \dot{q}_2 Y_1 + Y_4 = 0 \tag{6.3}$$

where $Y_1 = (2q_1 - T)$, $Y_2 = 2q_2$, $Y_3 = (\dot{D} - \dot{T}q_1)$ and $Y_4 = -\dot{T}q_2$. Now solving the equation (6.2) and (6.3), we get

$$\dot{q}_1 = -\frac{(Y_1 Y_3 + Y_2 Y_4)}{(Y_1^2 + Y_2^2)} \tag{6.4}$$

At $\xi_1 = \xi_1^{(H)}$, two cases arise:

Case I: when $q_1 = 0$ and $q_2 = \sqrt{D}$, we have $Y_1 = 0$, $Y_2 = 2\sqrt{D}$, $Y_3 = \dot{D}$ and $Y_4 = -\dot{T}\sqrt{D}$. Hence from equation (6.4), we get

$$[\dot{q_1}]_{\xi_1=\xi_1^{(H)}} = \left[\frac{dq_1(\xi_1)}{d\xi_1}\right]_{\xi_1=\xi_1^{(H)}} = \frac{1}{2}\left[\frac{dT(\xi_1)}{d\xi_1}\right]_{\xi_1=\xi_1^{(H)}} \neq 0.$$

Case II: when $q_1 = 0$ and $q_2 = -\sqrt{D}$, we have $Y_1 = 0$, $Y_2 = -2\sqrt{D}$, $Y_3 = \dot{D}$ and $Y_4 = \dot{T}\sqrt{D}$. Hence from equation (6.4), we get

$$[\dot{q_1}]_{\xi_1=\xi_1^{(H)}} = \left[\frac{dq_1(\xi_1)}{d\xi_1}\right]_{\xi_1=\xi_1^{(H)}} = -\frac{1}{2}\left[\frac{dT(\xi_1)}{d\xi_1}\right]_{\xi_1=\xi_1^{(H)}} \neq 0.$$

Hence the theorem is proved.

6.4. Cusp Bifurcation

We have already noted that system (2.2) may possesses three interior equilibrium points for a suitable selection of parameter values, namely $E_{I1}(x_3^{'}, y_3^{'})$, $E_{I2}(x_3^{''}, y_3^{''})$ and $E_{I3}(x_3^{'''}, y_3^{'''})$. There are two potential scenarios that can unfold when we iteratively modify any parameter value: either E_{I1} coincides with E_{I2} or E_{I2} coincides with E_{I3}, leading to the occurrence of two saddle-node bifurcations. These two saddle-node bifurcation points give rise to two separate saddle-node bifurcation curves within a certain two-parameter bifurcation plane. Whenever those two saddle-node bifurcation curves collides at some specific parameter values, a cusp bifurcation occurs. In other words, cusp bifurcation is a dynamical state of the system wherein three interior equilibria converge and coincide. On the other hand, when a branch point curve meets with an saddle-node bifurcation curve in some certain two parametric bifurcation plane, the cusp bifurcation also occurs.

6.5. Bogdanov–Takens Bifurcation

For a suitable selection of parametric values, the system (2.2) exhibits a saddle-node bifurcation as well as a Hopf bifurcation. From these two bifurcation points, one can generate a saddle-node bifurcation curve and a Hopf bifurcation curve in a certain two parametric bifurcation plane. If the saddle-node bifurcation curve intersects with the Hopf-bifurcation curve, a new bifurcation develops, known as the Bogdanov-Takens bifurcation. A dynamical system typically experiences a Bogdanov-Takens (BT) bifurcation at an equilibrium point whenever the Jacobian matrix has a zero eigenvalue with multiplicity two.

7. Numerical Simulation

In this section, we conduct a series of numerical simulations to provide a visual representation of these local bifurcations and to analyze how various parameters influence the dynamical behavior of the system (2.2).

7.1. One parameter bifurcation diagram

Here, we systematically explore different bifurcation diagrams by varying a single parameter within the model system, providing us a comprehensive view of how the system's dynamics evolve with respect to the chosen parameter.

7.1.1. Impact of varying mortality coefficient of predator

First, we fixed the parameter values as $\{r = 1.73, K = 4, m_1 = 0.115, B = 0.66, c = 0.733, \xi_1 = 0.404, \xi_2 = 0.173, m_2 = 0.745\}$ and vary the natural mortality coefficient of predator h_1. From Fig.3, we observe that the system changes its stability when the interior equilibrium point E_I meets with the predator-free equilibrium point E_{x_1} at $h_1 = h_1^{(TC)} = 0.2335$. At this point, the unstable predator-free equilibrium point becomes stable and the stable interior equilibrium point vanishes, i.e., at $h_1 = h_1^{(TC)}$, a transcritical bifurcation occurs.

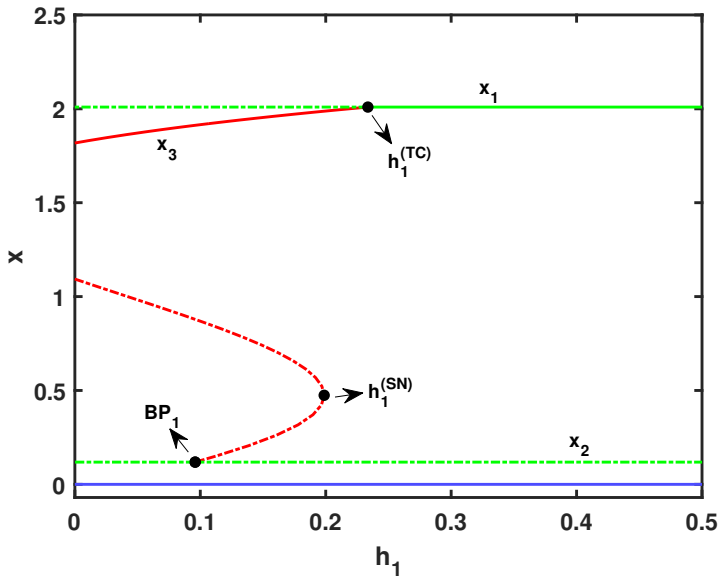

Figure 3: Bifurcation diagram of system (2.2) for the bifurcation parameter h_1. Green solid curve indicates the stable behavior of predator-free equilibrium point, the green dotted curve indicates the unstable behavior of predator-free equilibrium point. The upper and lower green curve denote the nature of predator-free equilibrium points E_{x_1} and E_{x_2} respectively. The red solid curve and red dotted curve respectively represent the stable and unstable behavior of the interior equilibrium point. The blue solid line represents the stable behavior of a species-free (trivial) equilibrium point.

Predator species go extinct at higher natural mortality coefficient h_1, particularly for $h_1 > h_1^{(TC)}$. This is ecologically legitimate, as higher mortality is always detrimental for any kind of species. On the other hand, we observe that two unstable interior equilibrium points approach and collide at $h_1 = h_1^{(SN)} = 0.1988$. At this point, a saddle-node bifurcation occurs. Again one unstable interior equilibrium point E_I meets with the unstable predator-free equilibrium point E_{x_2} at $BP_1 = 0.0959$. Due to the emergence of two distinct branches of unstable equilibrium points of the system, the point BP_1 is called the branch point. It is also observed that when $h_1 < BP_1$, system (2.2) has one stable and one unstable interior equilibrium point, two unstable predator-free equilibrium points, and one stable trivial equilibrium point. When $BP_1 < h_1 < h_1^{(SN)}$, one stable and two unstable interior equilibrium points, two unstable predator-free equilibrium points, and one stable trivial equilibrium point are present in the system. For $h_1^{(SN)} < h_1 < h_1^{(TC)}$, the system contains one stable interior equilibrium point, two unstable predator-free equilibrium points and one stable trivial equilibrium point. One stable and one unstable predator-free equilibrium points and one stable trivial equilibrium point are present when $h_1 > h_1^{(TC)}$.

When the natural mortality coefficient of predator is low, in particular if $h_1 < h_1^{(TC)}$, a situation of bi-stability arises between the interior equilibrium point and the trivial equilibrium point. Under these conditions, the survival of both species relies on their initial population sizes. In other words, at initial stage if the population size of both species are small, it may lead to a challenging for the coexistence of both species and if the population size of both species are large, there may exist a possibility for survival of both species. For $h_1 > h_1^{(TC)}$, the bi-stability phenomenon is observed between the predator-free equilibrium point and the trivial equilibrium point. In this scenario, the predator species always becomes extinct. To avoid complications, we only plot the changes of prey biomass with respect to changing h_1.

7.1.2. Impact of toxicity coefficient of predator

Next, we consider another bifurcation parameter ξ_2, which denotes the toxicity coefficient of predator species. First, we set the parameter values as $\{r = 1.73, K = 4, m_1 = 0.115, B = 0.66, c = 0.733, h_1 =$

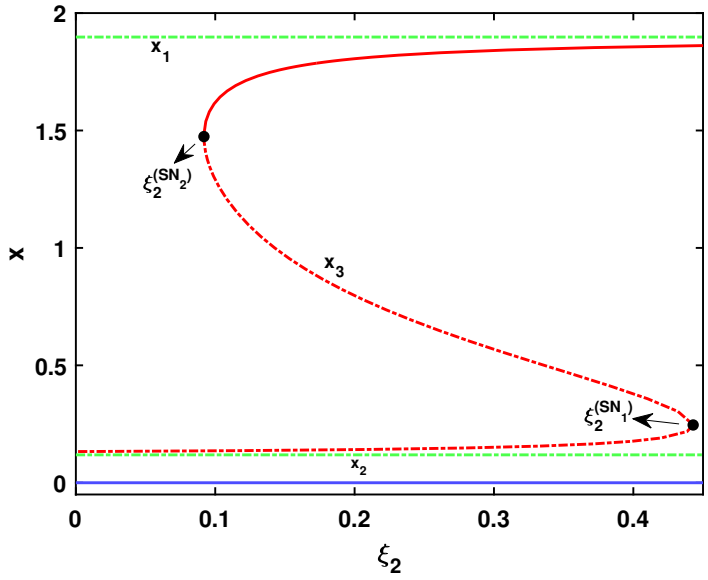

Figure 4: Bifurcation diagram of system (2.2) for the bifurcation parameter ξ_2. Green dotted curve indicates the unstable behavior of predator-free equilibrium point. The upper and lower green curve denotes the nature of predator-free equilibrium points E_{x_1}, E_{x_2} respectively. The red solid curve and red dotted curve represent the stable and unstable behavior of interior equilibrium point respectively. The blue solid line represents the stable behavior of trivial equilibrium point.

$0.107, \xi_1 = 0.45, m_2 = 0.745\}$ and vary the predator toxic parameter ξ_2. The resulting bifurcation diagram is depicted in Fig.4. From the figure, we observe that two unstable interior equilibrium points approach and collide at $\xi_2 = \xi_2^{(SN_1)} = 0.4429$. Furthermore, we observe similar type of scenario where one stable and one unstable interior equilibrium point approach and collide at $\xi_2 = \xi_2^{(SN_2)} = 0.0919$. Consequently, the system displays two saddle-node bifurcations precisely at the points $\xi_2 = \xi_2^{(SN_1)}$ and $\xi_2 = \xi_2^{(SN_2)}$. Considering the overall dynamics, it becomes evident that when $\xi_2 < \xi_2^{(SN_2)}$, the system (2.2) contains one unstable interior equilibrium point, two unstable predator-free equilibrium points, and one stable trivial equilibrium point. As ξ_2 falls within the range $\xi_2^{(SN_2)} < \xi_2 < \xi_2^{(SN_1)}$, the system displays one stable and two unstable interior equilibrium points, along with two unstable predator-free equilibrium points and one stable trivial equilibrium point. For $\xi_2 > \xi_2^{(SN_1)}$, the system includes one stable interior equilibrium point, two unstable predator-free equilibrium points, and one stable trivial equilibrium point.

When the coefficient of toxicity on predator species is small, precisely when $\xi_2 < \xi_2^{(SN_2)}$, both the predator and prey species struggle to maintain their survival. It is indeed surprising that a lower toxicity level for the predator can have a negative impact on ecological diversity. This outcome is also non-intuitive, as one might expect that reducing toxicity would lead to a more favorable environment for species to coexist. The primary explanation for this phenomenon lies in the fact that at lower toxicity levels, the predator's biomass tends to increase. As a consequence, the predation pressure on the prey species also intensifies, leading to a significant decrease in prey biomass. The absence of prey ultimately leads to the extinction of the predator species as well. On the other hand, if $\xi_2 > \xi_2^{(SN_2)}$, a bi-stability phenomenon emerges between the interior equilibrium point and the trivial equilibrium point. In such circumstances, the survival of both species are depends on their initial population sizes. In other words, during the initial stage when the population size of both species are small, it can create difficulties for their coexistence. Conversely, during the initial stage when the populations of both species are large, there is a possibility for survival of both species. To avoid complexity, we just plot the changes of prey biomass with respect to ξ_2.

7.1.3. Impact of toxicity coefficient of prey

Now, we consider another bifurcation parameter ξ_1 which denotes the coefficient of toxicity on prey species. Firstly we fixed the parameter values at $\{r = 1.73, K = 4, m_1 = 0.115, B = 0.66, c = 0.733, h_1 = 0.107, \xi_2 = 0.86, m_2 = 0.745\}$ and continuously change the toxic parameter ξ_1. From the Fig.5 we observe that stable interior equilibrium point loses stability when $\xi_1 = \xi_1^{(H)} = 1.8016$ and Hopf bifurcation occurs. To establish the direction of the Hopf bifurcation We numerically compute the first Lyapunov coefficient, which exhibits a positive value. This outcome indicates that the Hopf bifurcation is of subcritical type, resulting in the emergence of unstable bifurcating limit cycles. The unstable limit cycle shown in Fig.6. Once more, two unstable interior equilibrium points move closer and intersect at $\xi_1 = \xi_1^{(SN_1)} = 1.9757$, resulting in the occurrence of a saddle-node bifurcation. Again one unstable interior equilibrium point E_I meets with unstable predator-free equilibrium point E_{x_2} at $BP_1 = 1.6863$. The presence of two separate branches of unstable equilibrium points from BP_1 in the system, known as a branch point. On the other hand, two unstable predator-free equilibrium points E_{x_1}, E_{x_2} approach and collide at $\xi_1 = \xi_1^{(SN_2)} = 3.5477$ and saddle-node bifurcation occurs. It is also observed that when $\xi_1 < BP_1$, the system (2.2) contains two unstable predator-free equilibrium points, one stable interior equilibrium point and one stable trivial equilibrium point. When $BP_1 < \xi_1 < \xi_1^{(H)}$, one stable and unstable interior equilibrium points, two unstable predator-free equilibrium points, and one stable trivial equilibrium point are present for the system. Two unstable predator-free equilibrium points, two unstable interior equilibrium points and one stable trivial equilibrium point are present when $\xi_1^{(H)} < \xi_1 < \xi_1^{(SN_1)}$. For $\xi_1^{(SN_1)} < \xi_1 < \xi_1^{(SN_2)}$, the system contains two unstable predator-free equilibrium points, one stable trivial equilibrium point. When $\xi_1 > \xi_1^{(SN_2)}$, the system (2.2) contains only one stable trivial equilibrium point.

When the coefficient of toxicity on prey species is small i.e., $\xi_1 < \xi_1^{(H)}$, a bi-stability phenomenon emerges between the interior equilibrium point and trivial equilibrium point. In such scenarios, the survival of both species are depends on their initial population sizes. In other words, in the early stages, if both species have small population sizes, it could lead to a challenging for the coexistence of both species. Conversely, if both species have large initial population sizes, then there exist a possibility for survival of both species. When $\xi_1 > \xi_1^{(H)}$, the prey and predator species face extinction which is ecologically intuitive and meaningful.
To avoid complications, we only plot the changes in prey biomass with respect to changing ξ_1.

7.1.4. Impact of strong Allee effect

Next, we consider the bifurcation parameter m_1 which represents the strong Allee threshold value of prey species. At first, we fixed the parameter values at $\{r = 1.73, K = 4, B = 0.66, c = 0.733, h_1 = 0.107, \xi_1 = 0.45, \xi_2 = 0.173, m_2 = 0.745\}$ and vary the strong Allee threshold value m_1.

From the Fig.7, we observe that one stable and one unstable interior equilibrium point approach and collide at $m_1 = m_1^{(SN_1)} = 0.3471$. On the other hand, two unstable predator-free equilibrium point approach and collide at $m_1 = m_1^{(SN_2)} = 0.6672$. At the points $m_1 = m_1^{(SN_1)}$ and $m_1^{(SN_2)}$, saddle-node bifurcation occurs. Again one unstable interior equilibrium point meets with unstable predator-free equilibrium point E_{x_2} at $BP_1 = 0.1280$. This point is classified as a branch point due to the emergence of two distinct branches of unstable equilibrium points in the system. It is observed that when $m_1 < BP_1$, the system (2.2) contains one stable and two unstable interior equilibrium points, two unstable predator-free equilibrium points, one stable trivial equilibrium point. When $BP_1 < m_1 < m_1^{(SN_1)}$, one stable and one unstable interior equilibrium point, two unstable predator-free equilibrium points, one stable trivial equilibrium point are present for the system. Two unstable predator-free equilibrium points, one stable trivial equilibrium point are present when $m_1^{(SN_1)} < m_1 < m_1^{(SN_2)}$. When $m_1 > m_1^{(SN_2)}$, the system contain only stable trivial equilibrium point.

When the strong allee parameter of prey species is small i.e., $m_1 < m_1^{(SN_1)}$, a bi-stability phenomenon arises between the interior equilibrium point and trivial equilibrium point. Under such circumstances, the existence of both species depends on their initial population sizes. In other words, during the initial phases, if both species start with small populations, it might create challenges for their coexistence. Conversely, if both species commence with larger population sizes, the chance for the survival of both species increases.

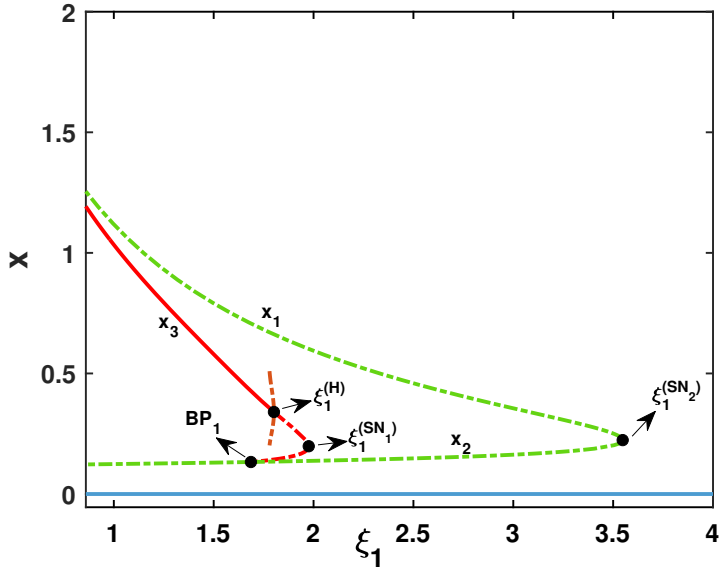

Figure 5: Bifurcation diagram of the system (2.2) for the bifurcation parameter ξ_1. Green dotted curve indicates unstable behavior of predator-free equilibrium point. The upper and lower green curve denote the nature of predator-free equilibrium points E_{x_1}, E_{x_2} respectively. The red solid curve and red dotted curve represent the stable and unstable behaviour of interior equilibrium point respectively. The orange dotted curve represents the unstable limit cycle. The blue solid line represents the stable behavior of species-free (trivial) equilibrium point.

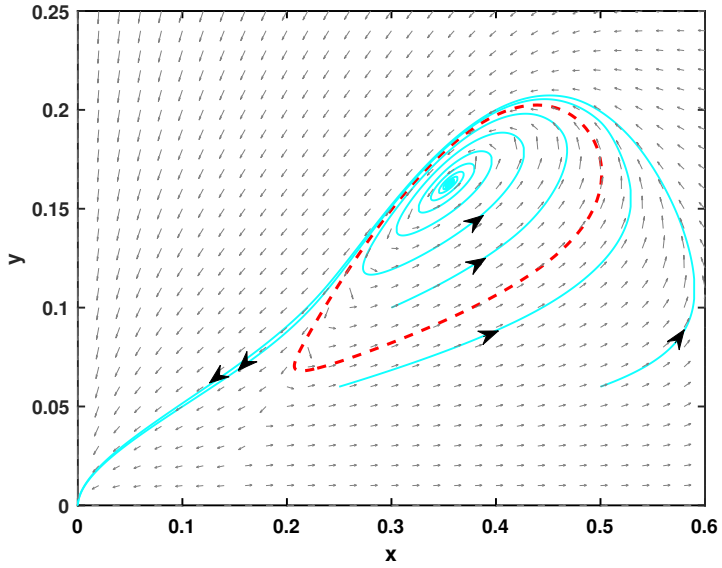

Figure 6: Phase portrait of the proposed model system showing the presence of unstable limit cycle. Red dotted curve represents unstable limit cycle. The light blue curve represents the trajectories that start from the different values of x, y at initial time ($t = 0$).

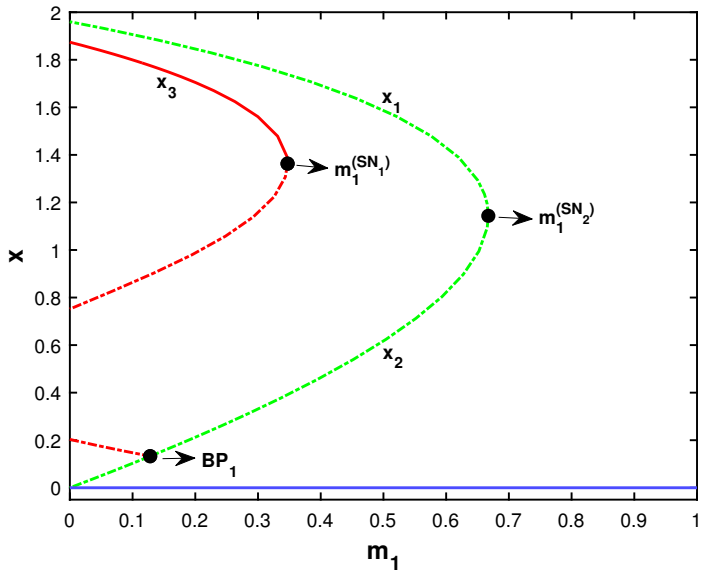

Figure 7: Bifurcation diagram of system (2.2) for the bifurcation parameter m_1. Green dotted curve indicates the unstable behaviour of predator-free equilibrium point. The upper and lower green curve denote the nature of predator-free equilibrium points E_{x_1}, E_{x_2} respectively. The red solid curve and red dotted curve represent the stable and unstable behaviour of interior equilibrium point respectively. The blue solid line represents the stable behavior of trivial equilibrium point.

When $m_1 > m_1^{(SN_1)}$, the prey and predator species face extinction. This holds ecological significance. To avoid complications, we only plot the changes of prey biomass with respect to changing strong allee parameter m_1.

7.2. *Two parametric bifurcation diagram and phase portraits*

We methodically investigate bifurcation diagrams by altering a pair of parameters within the model system. This approach grants us a comprehensive understanding of how the dynamics of the system transform in relation to the selected parameter changes.

7.2.1. *Bifurcation analysis for toxicity coefficient of prey and toxicity coefficient of predator*

Firstly, we have introduced the coefficient of toxicity on predator species in the presence of coefficient of toxicity on prey species to analyze the system (2.2). Due to the fact that it is very challenging to represent all possible bifurcations in a single framework, we therefore, identify the coefficient of toxicity on prey species ξ_1 and the coefficient of toxicity on predator species ξ_2 as important parameters for the bifurcation diagram. To better understand the dynamics of the system (2.2), we draw two parametric bifurcation diagram in $\xi_1-\xi_2$ plane and fixed all other parameters at $\{r = 1.73, K = 4, B = 0.66, c = 0.733, h_1 = 0.107, m_1 = 0.115, m_2 = 0.745\}$. Fig.8 displays the equivalent bifurcation diagram. Two saddle-node bifurcation curve intersects at the point $CP_1(1.3483, 0.6350)$ and subsequently, the curves vanish. At the point $CP_2(1.6864, 0.6903)$, an another saddle-node bifurcation curve intersects with the branch point curve and subsequently, the saddle-node bifurcation curve disappear. At the point CP_1, CP_2 cusp bifurcation occurs. One saddle-node bifurcation curve and one Hopf bifurcation curve intersects at the point $BT_1(1.2752, 0.5986)$ and consequently, the Hopf bifurcation curve disappear. Another saddle-node bifurcation curve intersects with the Hopf bifurcation curve at the point $BT_2(2.9905, 2.4453)$, leading to the disappearance of the Hopf bifurcation curve. Bogdanov-Takens bifurcation occurs at points BT_1 and BT_2. Within an ecological system, it is important to note that the toxicity coefficient for predator species does not exceed the coefficient of toxicity on prey species, keeping it in mind the entire $\xi_1 - \xi_2$ parametric plane is divided by five bifurcation curve, one branch point curve and black dotted curve into eight sub-regions, designated as R_1, R_2, R_3, R_4,

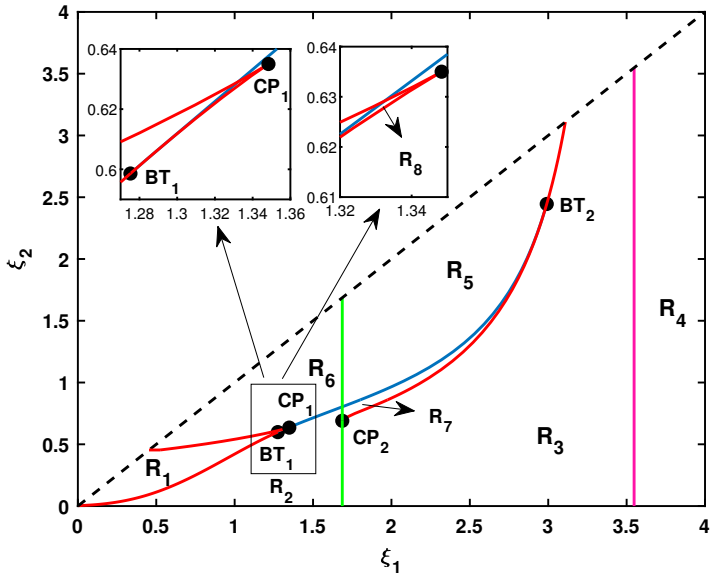

Figure 8: Two parametric bifurcation diagram of system (2.2) in $\xi_1 - \xi_2$ plane. Red solid curve reprsents the saddle-node bifurcation curves for the interior equilibrium points. Blue solid curve represents the Hopf bifurcation curve for interior equilibrium points. Pink solid curve represents the saddle node bifurcation curve for predator-free equilibrium points. Green solid curve represents the branch point curve. In black dotted curve the coefficient of toxicity on both species are same.

R_5, R_6, R_7 and R_8, which are shown in Fig.8. In the region R_1, the system (2.2) has three interior equilibrium points among them one is stable and the other two are unstable, two predator-free unstable equilibrium points, and one stable trivial equilibrium point. When we move from the R_1 region to both R_2 and R_6 region, two interior equilibrium points disappear through saddle-node bifurcation curve. In the region R_2, one unstable interior equilibrium point, two unstable predator-free equilibrium points, and one stable trivial equilibrium point are present. One stable interior equilibrium point, two unstable predator-free equilibrium points, and one stable trivial equilibrium point are present in the R_6 region. Conversely, when transitioning from the R_1 region to the R_8 region, the stable interior equilibrium point undergoes a loss of stability due to a Hopf bifurcation curve. Within region R_8,there are three unstable interior equilibrium points, two unstable predator-free equilibrium points, and one stable trivial equilibrium point. When we enter from the R_2 region to R_3 region, one unstable interior equilibrium point disappears through the branch point curve. In the region R_3, two unstable predator-free equilibrium points and one stable trivial equilibrium point are present. When we move from the region R_3 to R_7 region then two interior equilibrium points appear through saddle-node bifurcation curve. Two unstable interior equilibrium points and two unstable predator-free equilibrium points and one stable trivial equilibrium point are present in the region R_7. Conversely, during the transition from region R_3 to region R_4, two predator-free equilibrium points disappear by saddle-node bifurcation curve. The region R_4 consists of only one trivial stable equilibrium point. When we move from region R_3 to region R_5, a saddle-node bifurcation curve gives rise to the emergence of two interior equilibrium points. In the region R_5 the system (2.2) has two interior equilibrium points among them one is stable and the other one is unstable, two predator-free unstable equilibrium points, and one stable trivial equilibrium point.

Presently, our aim is to draw phase portraits of the system (2.2). This will be achieved by choosing the value of the parameter ξ_1 and ξ_2 from each region,while keeping the remaining parameter values at $\{r = 1.73, K = 4, B = 0.66, c = 0.733, h_1 = 0.107, m_1 = 0.115, m_2 = 0.745\}$. Fig.9 and Fig.10 represent the required phase portraits. From analyzing these phase portraits, it is evident that a bi-stability phenomenon arises between the interior equilibrium point and trivial equilibrium point within the region R_1,R_5 and R_6. In such scenarios, the survival of both species depends on their initial population size. Conversely, within

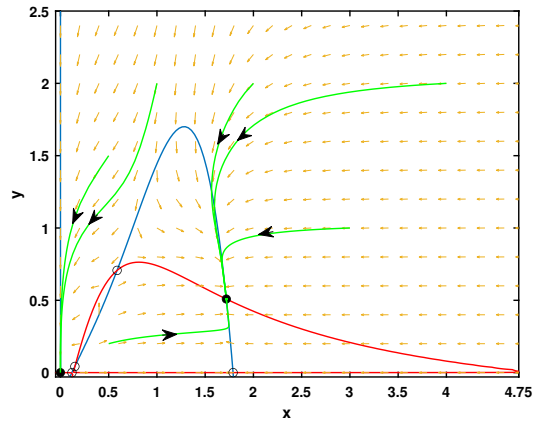

(a) For the Region R_1, where we take $\xi_1 = 0.5, \xi_2 = 0.3$

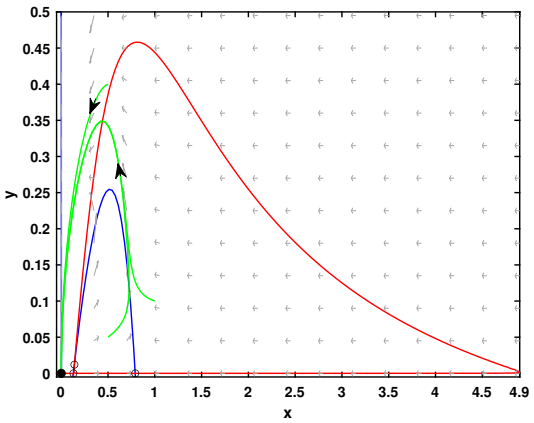

(b) For the region R_2, where we take $\xi_1 = 1.5, \xi_2 = 0.5$

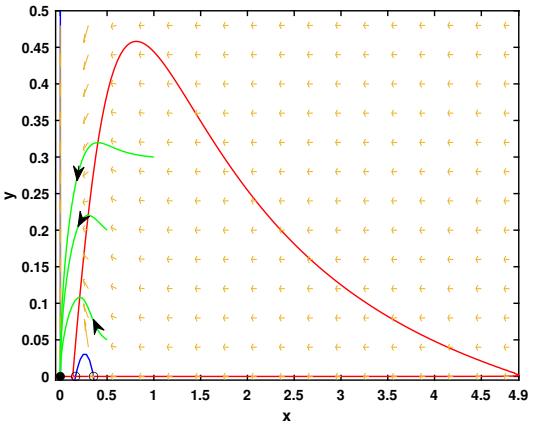

(c) For the region R_3, where we take $\xi_1 = 3, \xi_2 = 0.5$

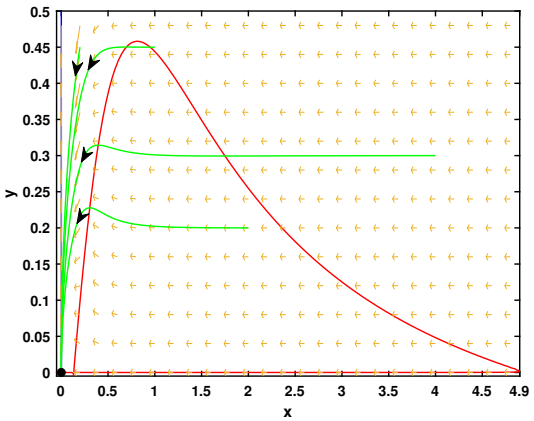

(d) For the region R_4, where we take $\xi_1 = 3.9, \xi_2 = 0.5$

Figure 9: Phase portrait of the system (2.2) for the region R_1, R_2, R_3 and R_4. Red solid curve and blue solid curve represent the predator nullcline and prey nullcline respectively. The green solid curve represents the trajectories that start from the different values of x, y at initial time ($t = 0$). The black dot point represents the stable behavior of equilibrium points, and the black circle point represents the unstable behavior of equilibrium points of the system (2.2) and the vector field can be drawn in each figure.

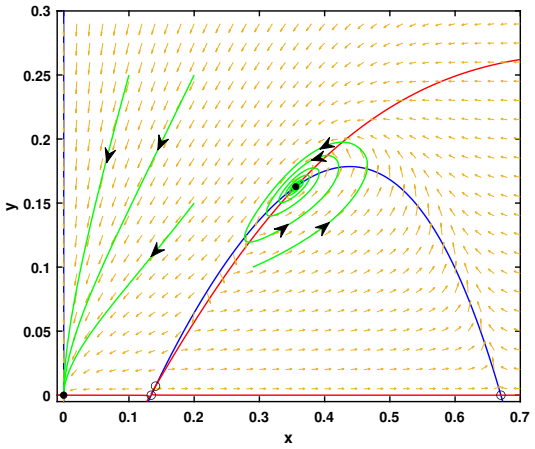

(a) For the region R_5, where we take $\xi_1 = 1.78, \xi_2 = 0.86$

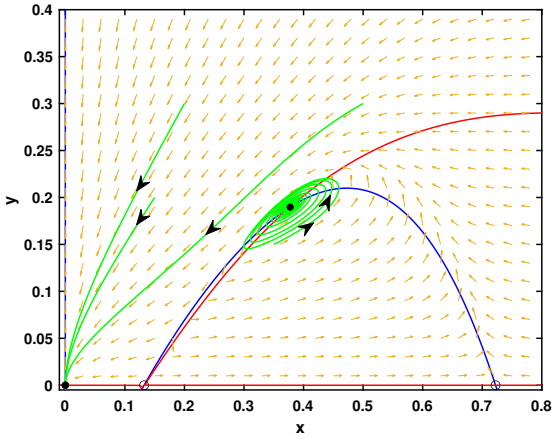

(b) For the region R_6, where we take $\xi_1 = 1.65, \xi_2 = 0.79$

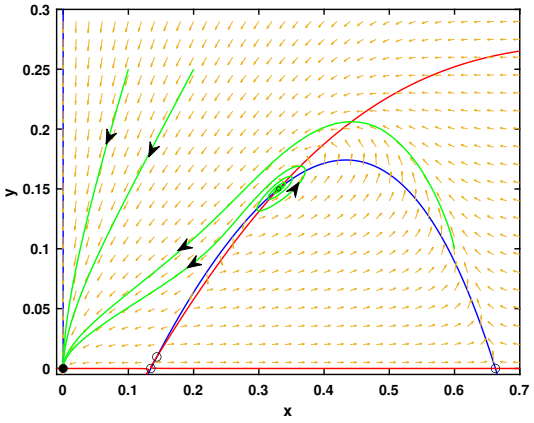

(c) For the region R_7, where we take $\xi_1 = 1.8, \xi_2 = 0.85$

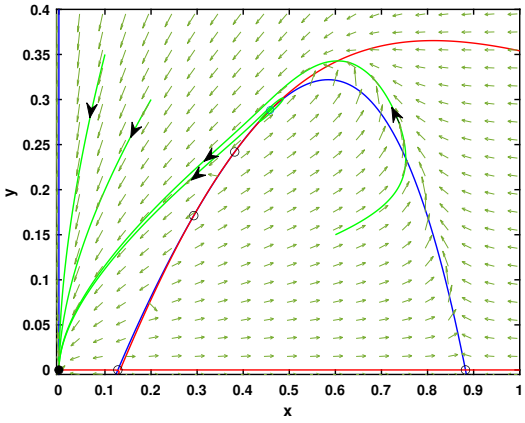

(d) For the region R_8, where we take $\xi_1 = 1.329, \xi_2 = 0.627$

Figure 10: Phase portrait of the system (2.2) for the region R_5, R_6, R_7 and R_8. Red solid curve and blue solid curve represent the predator nullcline and prey nullcline respectively. The green solid curve represents the trajectories that start from the different values of x, y at initial time ($t = 0$). The black dot point represents the stable behaviour of equilibrium points, and the black circle point represents the unstable behaviour of equilibrium points of the system (2.2) and the vector field can be drawn in each figure.

the regions R_2, R_3, R_4, R_7, and R_8, both the predator and prey species face extinction.

7.2.2. Bifurcation analysis for the toxicity coefficient of prey and the strong Allee parameter

For analyzing the system (2.2) in another way, we introduced the coefficient of toxicity on prey species ξ_1 and the strong Allee parameter m_1 for the bifurcation diagram. Two parametric bifurcation diagram in the $\xi_1 - m_1$ plane is drawn to help us better understand the dynamics of the system (2.2) and fixed all other parameters at $\{r = 1.73, K = 4, B = 0.66, c = 0.733, h_1 = 0.107, \xi_2 = 0.86, m_2 = 0.745\}$. The corresponding bifurcation diagram is shown in Fig.11. A saddle-node bifurcation curve intersects with the Hopf bifurcation curve at $BT_3(1.4489, 0.1430)$ and another saddle-node bifurcation curve intersects with the Hopf bifurcation curve at $BT_4(6.1921, 0.0675)$. At the points BT_3, BT_4 Bogdanov-Takens bifurcation occurs. On the other hand, a saddle-node bifurcation curve intersects with branch point curve at $CP_3(2.5765, 0.1056)$. At this point cusp bifurcation occurs. Presently, the complete $\xi_1 - m_1$ parameter plane is partitioned into six distinct subregions denoted as W_1, W_2, W_3, W_4, W_5, and W_6, achieved by the interaction of three bifurcation curves and one branch point curve, which shows in Fig.11. In the region W_1, the system (2.2) has only stable

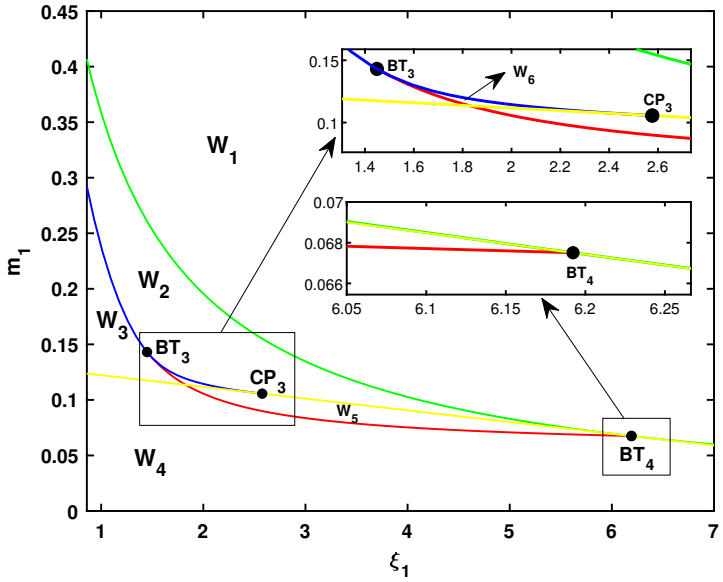

Figure 11: Two parametric bifurcation diagram of system (2.2) in $\xi_1 - m_1$ plane. Green solid curve represents saddle-node bifurcation curve for the predator-free equilibrium points. Red solid curve represents the Hopf bifurcation curve for interior equilibrium points. Blue solid curve represents saddle-node bifurcation curve for the interior equilibrium points. Yellow solid curve represents branch point curve.

trivial equilibrium point. As we move from the region W_1 to region W_2, two predator-free equilibrium points emerge due to a saddle-node bifurcation curve. Two unstable predator-free equilibrium points and one stable trivial equilibrium point are present in the region W_2. When we move from the region W_2 to W_3 region then two interior equilibrium points are appear through saddle-node bifurcation curve. In the region W_3 one stable and one unstable interior equilibrium points, two unstable predator-free equilibrium points, one stable trivial equilibrium point are present. When we shift from the region W_3 to W_4 region, an unstable interior equilibrium point vanishes along the branch point curve. One stable interior equilibrium point, two unstable predator-free equilibrium points, one stable trivial equilibrium points are present in the region W_4. When we enter from the region W_4 to W_5, the stable interior equilibrium point undergoes a loss of stability along the Hopf bifurcation curve. In the region W_5, one unstable interior equilibrium point, two unstable predator-free equilibrium points , one stable trivial equilibrium point are present. When we move from the region W_2 to W_6, two interior equilibrium point appear through saddle-node bifurcation curve. In the region W_6, the system (2.2) has two unstable interior equilibrium points, two unstable predator-free equilibrium points and one stable interior equilibrium point.

7.2.3. Bifurcation analysis for coefficient of toxicity of predator species and strong Allee parameter

To explore the system (2.2) from a different perspective, we introduced the toxicity coefficient on the predator species as ξ_2 and the strong Allee parameter m_1 into the bifurcation diagram. Two parametric bifurcation diagrams in the $\xi_2 - m_1$ plane have been constructed to enhance our comprehension of the dynamics exhibited by the system (2.2) and fixed all other parameters at $\{r = 1.73, K = 4, B = 0.66, c = 0.733, h_1 = 0.107, \xi_1 = 0.45, m_2 = 0.745\}$. The corresponding bifurcation diagram is shown in Fig.12. Three bifurcation curves and one branch point curve, as illustrated in Fig.12,partition the complete $\xi_2 - m_1$ parametric plane into six distinct subregions, labeled as G_1, G_2, G_3, G_4, G_5, and G_6.

In the region G_1 the system (2.2) has only a stable trivial equilibrium point. When we move from the region G_1 to G_2, two predator-free equilibrium points appear through the saddle-node bifurcation curve. Two unstable predator-free equilibrium points and one stable trivial equilibrium point are present in the region G_2. Two interior equilibrium points arise along a saddle-node bifurcation curve as we migrate from

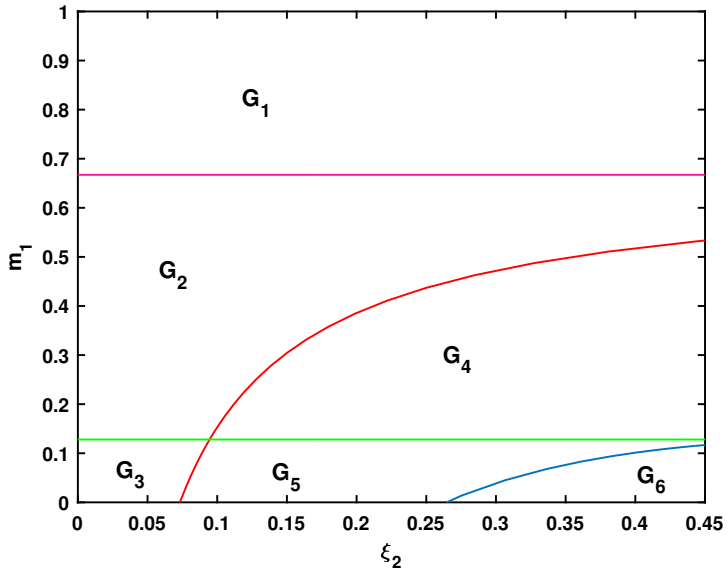

Figure 12: Two parametric bifurcation diagram of the system (2.2) in $\xi_2 - m_1$ plane. Red and blue solid curve represent two saddle-node bifurcation curve for interior equilibrium points. Pink solid curve represents saddle-node bifurcation curve for predator-free equilibrium points. Green solid curve represents branch point curve.

the region G_2 to G_4 . In the region G_4, two unstable predator-free equilibrium points, one stable and one unstable interior equilibrium point and one stable trivial equilibrium point are present. When we enter from the region G_2 to G_3, one interior equilibrium point appears through the branch point curve. Two unstable predator-free equilibrium points, one unstable interior equilibrium point and one stable trivial equilibrium point are present in the region G_3. Two interior equilibrium points arise along a saddle-node bifurcation curve as we migrate from the region G_3 to G_5 region . In the region G_5, the system (2.2) has two unstable predator-free equilibrium points, two unstable and one stable interior equilibrium point and one stable trivial equilibrium point. When we move from the region G_5 to G_6 then two interior equilibrium points disappear through saddle-node bifurcation curve. Two unstable predator-free equilibrium points, one stable interior equilibrium point, and one stable trivial equilibrium point are present in the region G_6.

7.3. Basins of attraction

The basin of attraction refers to the set of initial conditions from which a particular equilibrium state of the system can be attained in long time run. In simpler terms, it is the region in the state space where the dynamics of the system will lead to a specific outcome. Understanding the basin of attraction is crucial for predicting the long-term behavior of system (2.2). It helps us in determining the equilibrium state that the system will reach for a given set of initial conditions, and how sensitive the system is to changes in those initial conditions. In order to depict the basin of attraction for the system, we initially assign the parameter values as: $\{r = 1.73, K = 4, B = 0.66, c = 0.733, h_1 = 0.107, \xi_2 = 0.86, m_2 = 0.745, \xi_1 = 1.79, m_1 = 0.115\}$. For this particular set of parameter set, the system contains one stable interior equilibrium point, one unstable interior equilibrium point, two unstable predator free equilibrium point and one stable trivial equilibrium point. Therefore, one can observe a bi-stability between an interior equilibrium point and a trivial equilibrium point, and the corresponding basin of attraction is depicted in Fig.13a. This figure illustrates that despite having a high initial population biomass, both the prey and predator populations can still be at risk of extinction. A small region can be identified within the state space where both the prey and predator populations have the potential to survive. Next, we examine the alterations in these stability regions as the toxicity coefficient of the prey species (ξ_1) is varied. When ξ_1 is reduced to $\xi_1 = 1.5$,

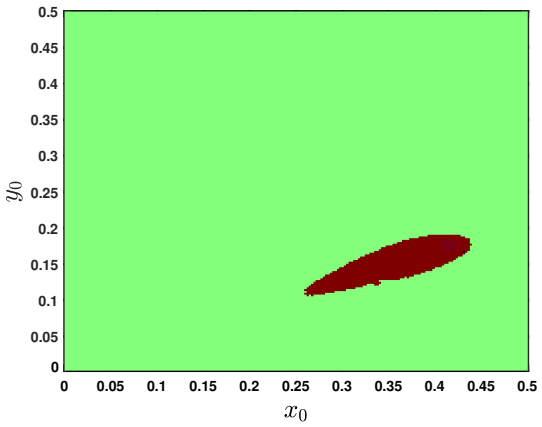

(a) Basins of attraction-I

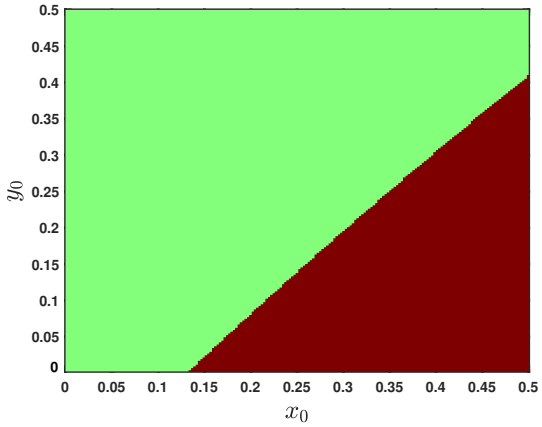

(b) Basins of attraction-II

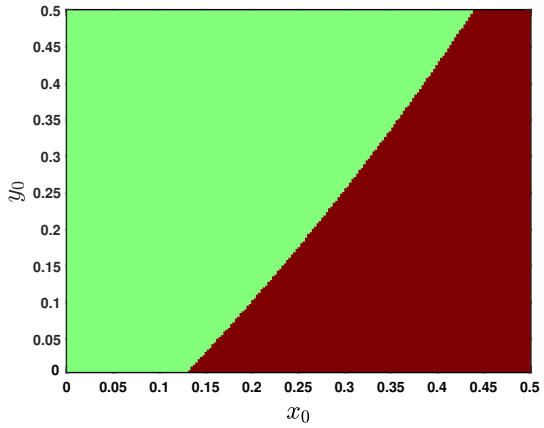

(c) Basin of attraction-III

Figure 13: Basin of attractions of system (2.2). Green area denotes the basin of attraction for the trivial equilibrium point and the brown area denotes the basin of attraction for an interior equilibrium point of the system.

the stability region of the coexistence steady state expands as depicted in Fig.13b. In such a scenario, the presence of an adequately high initial prey biomass alone becomes enough to facilitate coexistence. Upon further decreasing of ξ_1 to $\xi_1 = 1.1$, an even more extensive region becomes evident in Figure 13c. From an ecological perspective, this observation implies that reducing the toxicity coefficient for the prey species has a positive impact on the survival of both the prey and predator populations. This ecological adjustment aligns with the principles of biodiversity preservation and stability within the ecosystems.

8. Discussion

Understanding the dynamical complexity of the ecosystem and finding the ecological components that influence this complexity are key characteristics of ecological study. Several mathematical models have been developed in recent years to investigate different types of ecological processes under various environmental limitations. The predator-prey interaction model is one example of an ecological model. The underlying factors that significantly contribute to the establishment of the community structure can be identified by thoroughly examining a predator-prey model with a variety of biological or physiological features as well as the preservation of biodiversity. For both prey and predator, toxicity is one such physiological component.

Toxicants in prey species might cause predator species to change their behaviour. In the present work, a predator-prey model is proposed which takes into account the impact of toxicity on both reproduction and the mortality rate of prey and predator species. In order to create more plausible dynamics, the proposed model includes the strong Allee effect in prey species and Holling type IV functional response.

First, we have shown the positivity and boundedness of solutions in a confined region $H \subseteq \mathbb{R}^2_+$, demonstrating the well-posedness of the proposed system. In addition to one trivial equilibrium point E_0, the system contains two predator-free equilibrium points E_{x_1} and E_{x_2}. For $r^2(k - m_1)^2 = 4k^2 m_1 r\xi_1$, those two predator-free equilibrium points collide at a single predator-free equilibrium point E_{x^*}. The existence and numbers of interior equilibrium point rely on a variety of factors that are discussed in section 4.2. Using the method of linear stability analysis, the local stability characteristics of the system are investigated in the vicinity of each equilibrium point. The trivial equilibrium point E_0 is always locally asymptotically stable which is discussed in the theorem 5.1. The stable and unstable behavior of predator-free equilibrium points E_{x_1} and E_{x_2} are discussed in theorem 5.2 and theorem 5.3. The stability characteristics of interior equilibrium points E_I are discussed in theorem 5.4. Throughout this study, significant attention is directed towards the coefficient of toxicity in predator species ξ_2, the coefficient of toxicity in prey species ξ_1, the natural mortality coefficient of predator h_1, and the strong Allee parameter m_1. As a result, we look at how the system dynamics are changed in quality with the variation of parameters ξ_1, ξ_2, h_1, and m_1. From numerical investigations, we have observed that the system undergoes two saddle-node bifurcations for the parameter ξ_2 and m_1; one transcritical bifurcation and one saddle-node bifurcation for the parameter h_1; one Hopf bifurcation and two saddle-node bifurcations for the parameter ξ_1. For a sufficient selection of parameter values, the system may exhibit a bi-stable phenomenon between the trivial equilibrium point and an interior equilibrium point. As the level of natural mortality of predator h_1 is increased, the predator species faces the higher risk of extinction. Likewise, when we increase the values of ξ_1 and m_1, the interior equilibrium points disappear, leading to the subsequent disappearance of predator-free equilibrium points. On the other hand, the higher level of ξ_2 promotes existence of interior equilibrium point which becomes locally asymptotically stable alongside another stable trivial equilibrium point. Additionally, we conducted an investigation of the two parametric bifurcations and found that the $\xi_1 - \xi_2$ and $\xi_1 - m_1$ parametric plane exhibits both a Bogdanov–Takens bifurcation and a Cusp bifurcation. We also discuss another two parametric bifurcation diagram in the $\xi_2 - m_1$ plane, which is discussed in section 7.2.3. The basin of attraction of equilibrium points when the system exhibit bi-stable phenomenon is also discussed in section 7.3. The detalied study of this kind of model has a thorough application in understanding the population dynamics in real life. As an example let us take the relationship between poisonous frogs and their predators in tropical rainforests. Poison dart frogs, like the golden poison frog, emit neurotoxins known as batrachotoxins. Although these toxins are accumulated through ingestion by diminutive invertebrates such as ants and mites, these poisons originate from the alimentation of these infinitesimal creatures. These frogs' brilliant colours serve as an aposematic signal, alerting prospective predators to their toxicity. The pervasive effects which these toxic substances exert on the complex interrelationships between hunters and the hunted have been thoroughly investigated by researchers [22]. They discovered that predator species like snakes and birds who tried to eat the poisoned frogs suffered severe physiological damage or even death as a result of the toxic substances. This puts predator under significant selection pressure to avoid feeding on these brilliantly coloured frogs, resulting in a coevolutionary arms race between the poisonous frogs and their prospective predators.

Eating of toxic prey can have a substantial impact on predator populations in the wild. Research [11] showed that predatory fish that consumed poisonous zooplankton suffered slower development and higher mortality, resulting in alterations in the structure and function of the aquatic food web. These findings highlight the significance of knowing the effects of prey poisons on predator population and ecological dynamics. Toxic prey can have a variety of consequences for predators. It can, for example, alter predator behaviour, morphology, physiology, and developmental pathways [25]. It can also change predator-prey relationships, affecting community structure [34]. The model may be further enhanced for two prey, and one predator system in the future, which may be important for establishing community structure and preserving biological variety.

Acknowledgements

Souvick Karmakar is thankful to the Ministry of Social Justice and Empowerment, Government of India for providing Fellowship. Parvez Akhtar is thankful to the University Grants Commission, Government of India for providing JRF.

Data availability statement

The data used to support the findings of the study are available within the article.

Conflict of interest

The authors declare that they have no conflict of interest regarding this work.

References

[1] R. P. Agarwal, O. Bazighifan, and M. A. Ragusa, *Nonlinear neutral delay differential equations of fourth-order: oscillation of solutions*, Entropy, 23(2):129, 2021.
[2] B. Anderson, J. Jackson, and M. Sitharam, *Descartes' rule of signs revisited.* The American Mathematical Monthly 105(5):447–451, 1998.
[3] F. Chen, L. Chen, and X. Xie, *On a leslie–gower predator–prey model incorporating a prey refuge*, Nonlinear Analysis: Real World Applications, 10(5):2905–2908, 2009.
[4] F. Courchamp, L. Berec, and J. Gascoigne, *Allee effects in ecology and conservation*, OUP Oxford, 2008.
[5] B. K. Das, D. Sahoo, and G. P. Samanta, *Impact of fear in a delay-induced predator–prey system with intraspecific competition within predator species*, Mathematics and Computers in Simulation, 191:134–156, 2022
[6] A. Duro, V. Piccione, M. A. Ragusa, and V. Veneziano, *New enviromentally sensitive patch index-espi-for medalus protoco*, In AIP Conference Proceedings, volume 1637, pages 305–312. American Institute of Physics, 2014.
[7] W. H. Herbert, W. Wang, L. Han, and M. Zhien, *A predator–prey model with infected prey*, Theoretical population biology, 66(3):259–268, 2004.
[8] C. S. Holling, *Some characteristics of simple types of predation and parasitism1*, The canadian entomologist, 91(7):385–398, 1959.
[9] J. Huisman and F. J. Weissing, *Fundamental unpredictability in multispecies competition*, The American Naturalist, 157(5):488–494, 2001.
[10] M. Kot, *Elements of mathematical ecology*, Cambridge University Press, 2001.
[11] J. H. Landsberg, K. A. Lefebvre, and L. J. Flewelling, *Effects of toxic microalgae on marine organisms*, Toxins and biologically active compounds from microalgae, 2:379–449, 2014.
[12] A. J. Lotka, *Elements of physical biology*, Williams and Wilkins. Baltimore, Md, 1925.
[13] F. Messier, *Ungulate population models with predation: a case study with the north american moose*, Ecology, 75(2):478–488, 1994.
[14] J. Monod, *The growth of bacterial cultures*, Annual review of microbiology, 3(1):371–394, 1949.
[15] W. W. Murdoch, C. J. Briggs, and R. M. Nisbet, *Consumer-resource dynamics (MPB-36)*, Prince-ton University Press, 2013.
[16] J. D. Murray, *Mathematical Biology: II: Spatial Models and Biomedical Applications*, volume 3. Springer, 2003.
[17] L. Perko, *Differential equations and dynamical systems, volume 7*, Springer Science and Business Media, 2013.
[18] V. Piccione, M. A. Ragusa, V. Rapicavoli, and V. Veneziano, *Monitoring of a natural park through espi*, In AIP Conference Proceedings, volume 1978, page 140005. AIP Publishing LLC, 2018.
[19] S. Saha, A. Maiti, and G. P. Samanta, *A Michaelis-Menten predator–prey model with strong allee effect and disease in prey incorporating prey refuge*, International Journal of Bifurcation and Chaos, 28(06):1850073, 2018.
[20] N. Satra, S. Saha, G. Samanta, *Role of multiple time delays on a stage-structured predator–prey system in a toxic environment*, Mathematics and Computers in Simulation, 212:548–583, 2023.
[21] R. A. Saporito, M. A. Donnelly, P. Jain, H. M. Garraffo, F. T. Spande, and J. W. Daly, *Spatial and temporal patterns of alkaloid variation in the poison frog oophaga pumilio in costa rica and panama over 30 years*, Toxicon, 50(6):757–778, 2007.
[22] R. A. Saporito, M. A. Donnelly, R. A. Norton, H. M. Garraffo, F. T. Spande, and J. W. Daly, *Oribatid mites as a major dietary source for alkaloids in poison frogs*, Proceedings of the National Academy of Sciences, 104(21):8885–8890, 2007.
[23] S. Sharma and G. P. Samanta, *Dynamical behaviour of a two prey and one predator system*, Differential Equations and Dynamical Systems, 22(2):125–145, 2014.
[24] S. Sharma and G. P. Samanta, *A Leslie–Gower predator–prey model with disease in prey incorporating a prey refuge*, Chaos, Solitons and Fractals, 70:69–84, 2015.
[25] M. J. Sheriff and J. S. Thaler, *Ecophysiological effects of predation risk; an integration across disciplines*, Oecologia, 176:607–611, 2014.
[26] E. C. Pielou, *Mathematical ecology*, john wiley and sons, New York 1977.
[27] P. A. Stephens, W. J. Sutherland, and R. P. Freckleton, *What is the allee effect?*, Oikos, pages 185–190, 1999.
[28] Y. Takeuchi, Y. Oshime, and H. Matsuda, *Persistence and periodic orbits of a three-competitor model with refuges*, Mathematical biosciences, 108(1):105–125, 1992.
[29] D. Tilman, *Resource competition and community structure*, Princeton university press, 1982.

[30] V. Volterra, *Variazioni e fluttuazioni del numero d'individui in specie animali conviventi, volume 2*, Societ a anonima tipografica" Leonardo da Vinci", 1927.
[31] G. A. K. Van Voorn, L. Hemerik, M. P. Boer, and B. W. Kooi, *Heteroclinic orbits indicate overexploitation in predator–prey systems with a strong allee effect*, Mathematical biosciences, 209(2):451–469, 2007.
[32] J. Wang, J. Shi, and J. Wei, *Predator–prey system with strong allee effect in prey*, Journal of Mathematical Biology, 62(3):291–331, 2011.
[33] M. H. Wang and M. Kot, *Speeds of invasion in a model with strong or weak allee effects*, Mathematical biosciences, 171(1):83–97, 2001.
[34] J. S. Weis, G. Smith, T. Zhou, C. Santiago-Bass, and P. Weis, *Effects of contaminants on behavior: biochemical mechanisms and ecological consequences: killifish from a contaminated site are slow to capture prey and escape predators; altered neurotransmitters and thyroid may be responsible for this behavior, which may produce population changes in the fish and their major prey, the grass shrimp*, Bioscience, 51(3):209–217, 2001.